Theory of interfacial orientational relaxation spectroscopic observables

Zsolt Gengeliczki, Daniel E. Rosenfeld, and M. D. Fayer[a)]
Department of Chemistry, Stanford University, Stanford, California 94305, USA

(Received 20 January 2010; accepted 10 May 2010; published online 24 June 2010)

The orientational correlation functions measured in the time-resolved second-harmonic generation (TRSHG) and time-resolved sum-frequency generation (TRSFG) experiments are derived. In the laboratory coordinate system, the $\langle Y_l^m(\Omega_{\mathrm{lab}}(t))Y_2^m(\Omega_{\mathrm{lab}}(0))\rangle$ ($l=1,3$ and $m=0,2$) correlation functions, where the Y_l^m are spherical harmonics, describe the orientational relaxation observables of molecules at interfaces. A wobbling-in-a-cone model is used to evaluate the correlation functions. The theory demonstrates that the orientational relaxation diffusion constant is not directly obtained from an experimental decay time in contrast to the situation for a bulk liquid. Model calculations of the correlation functions are presented to demonstrate how the diffusion constant and cone half-angle affect the time-dependence of the signals in TRSHG and TRSFG experiments. Calculations for the TRSHG experiments on Coumarin C314 molecules at air-water and air-water-surfactant interfaces are presented and used to examine the implications of published experimental results for these systems. © *2010 American Institute of Physics*.
[doi:10.1063/1.3442446]

I. INTRODUCTION

Interfaces and surfaces play an important role in heterogeneous catalysis,[1,2] electrochemistry,[3] nanoscience,[4] atmospheric chemistry,[5,6] and biology.[7,8] Therefore, it is important to understand the special physical and chemical properties of such interfaces at the molecular level. Static and dynamic molecular properties of interfaces cannot be derived or estimated from bulk phase measurements, and techniques have been developed to determine the interfacial composition and orientation of molecules at interfaces.

Some of the most powerful tools for spectroscopic investigation of interfaces are second-harmonic generation (SHG) and sum-frequency generation (SFG) spectroscopies.[9,10] These techniques rely on the second-order nonlinear properties of interfaces. In contrast to most bulk phases, interfaces are noncentrosymmetric. Because of this fact, SHG and SFG can provide nearly interference-free measurements of interfacial spectroscopic properties.[11,12] One of the useful properties measured with these techniques is the equilibrium orientation of molecules at interfaces and surfaces.[11–14] SFG was also successfully used for *in situ* identification of reaction intermediates on nanoparticle catalysts both at atmospheric and high pressure.[11–13,15–17]

Although static measurements give invaluable insights into the structure of molecular interfaces, surface reactivity and transport phenomena cannot be described without understanding of the dynamical behavior. Molecular orientational relaxation affects the SFG and SHG signals and limited information can be obtained through the time-independent variations in signal intensities with respect to electric field polarizations.[18] To obtain detailed dynamical information, time-dependent versions of SFG and SHG spectroscopies have been developed in which either SFG or SHG are used as probes subsequent to an incident pump pulse.[19–23] These techniques are typically referred to as time-resolved second-harmonic generation (TRSHG) and time-resolved sum-frequency generation (TRSFG) spectroscopies. In any time-resolved method such as TRSHG or TRSFG, molecular orientational relaxation contributes to the measured time-dependence of the signals.[19,22,24,25] Such experiments are analogous to measurements of orientational relaxation dynamics of molecules in bulk liquids. The time-dependence of the interfacial molecular reorientation signal can provide information on the nature of orientational motions of molecules at an interface and permit comparison to the behavior of molecules in bulk liquids. In recent years, measurements have been made of the time scales of molecular reorientation and excited state population relaxation at the air-water interface with different pumping schemes.[23–28] The various pumping schemes typically differ in the polarization and frequency of the pump laser.

McGuire and Shen[23] applied an infrared pump to the OH stretch of interfacial water molecules, which was subsequently probed by SFG. Eisenthal and co-workers[24,25] demonstrated that electronic excitation causes a depletion in both the SHG and the SFG signals, and that reorientation of the molecules can be observed by following the recovery of the signal. The time-dependent signal is caused by the reorientation of the molecules at the interface and the electronic or vibrational lifetime relaxation. If the electronic or vibrational lifetime is long enough, the initial fast decay time constant can be assigned to the reorientation of the interfacial molecule. In many cases, the reorientational time constant is compared to the time constant measured in the bulk phase.[25]

Eisenthal and co-workers[24] have performed studies of the orientational relaxation of Coumarin 314 (C314) at the air-water interface using both TRSHG and TRSFG experiments. They assigned the extracted time constants to the

[a)]Electronic mail: fayer@stanford.edu.

"in-plane" and "out-of-plane" reorientation of the molecules at the interface. Their findings can be summarized in a few points: (1) the orientational dynamics can be isolated from the population relaxation due to a separation of timescales for the coumarin system and (2) the SHG signal recovery caused by the reorientational motion of the molecules is single exponential and there is a remaining bleach once the reorientation is complete. In principle, the recovery of the SHG signal should be biexponential if both the in-plane (change in the azimuthal angle) and the out-of-plane (change in the polar angle) motions are observed. Eisenthal and co-workers[27] stated that the two motions happen on a very similar time scale and they measure almost identical time constants. They directly compared the measured exponential decay time constants with the bulk phase orientational relaxation time constants. As will be derived in detail below, such a direct comparison is invalid due to a different relationship between the decay times and the orientational diffusion constants. In contrast to bulk liquids, observed interfacial orientational decay times are not directly related to the inverse of the orientational diffusion constant.

Recently, Nienhuys and Bonn[28] developed a numerical method for assigning rotational diffusion constants for the reorientation of molecules at the air-liquid interface studied by TRSFG experiments. For the hypothetical situation in which orientational relaxation is only allowed in the azimuthal angle (a one-dimensional random walk with cyclic boundary condition), the dynamic nonlinear susceptibilities are expressed analytically as exponential decays. However, for the physically realistic situation in which reorientation is allowed in both the azimuthal and polar angles, a number of specific cases are considered and the results are reported as numerical solutions. In their model, they assume a harmonic potential that governs the "out-of-plane motion" (change in the polar angle) of the molecules, while they treat the in-plane motion (change in the azimuthal angle) as a free rotation about the surface normal. The two types of motions are assumed to be decoupled, that is, the in-plane rotational diffusion constant does not depend on the out-of-plane orientation angle. The in-plane and out-of-plane reorientational dynamics can only be fully separated when the out-of-plane angle is restricted to a very narrow range.[28] In addition, because the framework for analyzing the out-of-plane motion in the TRSFG and TRSHG experimental data is numerical, it is difficult to obtain a broad understanding of the factors that influence the experimental observables.

None of the above studies determine which correlation functions are measured in the TRSHG and TRSFG experiments. Without knowledge of the correlation functions associated with a particular experiment, experimental observables cannot be calculated or simulated. Previously, there have been no analytical treatments of the spectroscopic observables of molecules undergoing orientational relaxation at interfaces that relate the observables to the orientational diffusion constants.

In the present paper, we analyze polarization selective TRSFG and TRSHG experimental observables in a comprehensive manner. First we will discuss which correlation functions are measured in these experiments. The electric-field-matter interactions differ in number and type from those in bulk phase polarization selective pump-probe experiments, and they include both resonant and nonresonant interactions. The correlation functions will be obtained in general for a well defined molecular symmetry. Then the results are made specific for a wobbling-in-a-cone model,[29–31] in which the orientational motion is restricted to a cone of angles. The wobbling-in-a-cone model allows us to express the time constant of the observed exponential decay as a function of the half-cone angle and to extract the orientational diffusion constant. The tilt angle of the cone relative to the interface normal is also included in the treatment. This general tilt angle permits the theory to treat cases in which the interfacial molecules can diffuse within a range of angles that is not centered on the surface normal. Model calculations are presented to illustrate the theoretical results.

The theory presented below shows that the observed orientational decays for surface selective nonlinear experiments are not directly related to the orientational diffusion constant. Therefore, the time constants of decays observed at interfaces cannot be directly compared to the time constant of decays measured in the bulk. The results presented here not only permit interfacial orientational diffusion constants to be obtained, but they also make it possible to extract information about the range of angles over which orientational relaxation occurs from the time-dependent measurements.

Data from the literature on C314 at the air-water[24,22] and air-water-surfactant[25,27] interfaces are analyzed and reinterpreted. While the orientational relaxation time constants at the air-water interface and in bulk water differ substantially, it is shown that the orientational diffusion constants are in fact the same within a small error. In addition, although the relaxation time constants at the air-water interface and the air-water-surfactant interface are almost the same, the surfactant reduces the orientational diffusion constant by a factor of approximately three. These results demonstrate that it is possible to extract detailed information on the influence of interfaces on molecular orientational dynamics by obtaining the orientational diffusion constants from the data.

II. THEORETICAL FRAMEWORK

Since one of the goals of this work is to relate interfacial orientational relaxation correlation functions to those measured for the bulk, we briefly review the observable for bulk orientational relaxation. Orientational dynamics of molecules in the isotropic liquid phase can be studied with pump-probe and fluorescence anisotropy experiments. The theory of these experiments is well understood.[32] The anisotropy of the orientational relaxation in the bulk phase is given by

$$r(t) = \frac{I_{\parallel}(t) - I_{\perp}(t)}{I_{\parallel}(t) + 2I_{\perp}(t)} = \frac{2}{5}C_2(t), \tag{1}$$

where $r(t)$ is the orientational anisotropy and $I_{\parallel}(t)$ and $I_{\perp}(t)$ are the components of the observable (probe pulse and fluorescence) measured parallel and perpendicular to the pump pulse, respectively.[33,34] $C_2(t)$ is the second-order Legendre polynomial orientational correlation function,[35]

$$C_2(t) = \langle P_2(\hat{\mu}(t)\hat{\mu}(0))\rangle, \quad (2)$$

where $\hat{\mu}$ is the transition dipole. For isotropic orientational diffusion of an ensemble of spherical rotors, the correlation function is a single exponential decay with time constant $\tau = 1/6D_{or}$ and rotational diffusion constant D_{or}, specifically

$$C_2(t) = e^{-6D_{or}t}. \quad (3)$$

This is a well known formula that can be derived by solving the isotropic diffusion equation.[36,37] Treatment has been presented for other molecular shapes such as oblate and prolate spheroids.[33,32]

Molecules can also undergo restricted rotational diffusion if the local environment is anisotropic, for example, in glassy materials,[31,38] macromolecules,[39,40] membranes,[41] and reverse micelles.[42] A model that has been widely used to describe these systems is wobbling-in-a-cone. The model involves a rigid rod with cylindrical symmetry whose cylindrical axis is confined within a conical volume, and the potential is uniform within the cone and infinite outside of the cone. This is referred to as the hard-wall cone model. The $C_2(t)$ correlation function can be expressed analytically and gives a single exponential decay to a nonzero constant. The magnitude of the constant is determined by the cone half-angle. Combining the decay time constant and the cone angle yields the orientational diffusion constant for motion within the cone. Szabo[33,43] presented comprehensive discussions of the wobbling-in-a-cone problem for probes embedded in macromolecules, and macroscopically oriented samples, such as uniaxial liquid crystals.[43] Pecora and Wang expressed the orientational correlation function in terms of spherical harmonics and gave a general and mathematically rigorous derivation of the $\langle Y_l^m(\Omega(t))Y_l^m(\Omega(0))\rangle$ $(l=1,2;\ m=0,1,2)$ correlation functions, which can be used as a template for employing the wobbling-in-a-cone-model in different types of experiments.[30] The wobbling-in-a-cone model has been extended to a "harmonic cone" in which the cone is a two-dimensional parabolic potential.[44]

Below, the necessary formalism for solving for the orientational relaxation component of TRSHG probe and TRSFG probe experiments will be derived. As this derivation is long and intricate we will begin with a brief outline. First, in Sec. II A, the electric-field-matter interactions which give rise to pump-SHG probe and pump-SFG probe signals will be formalized via diagrammatic perturbation theory. In Sec. II B, the tensorial nature of these interactions will be considered, resulting in general expressions for the orientational response functions. Given experimental conditions, the orientational correlation functions can be expanded in time correlation functions of spherical harmonics. The remainder of the work in Sec. II will be directed toward finding analytical expressions for the spherical harmonic correlation functions which contribute to the orientational response. Section II C will construct the angular coordinates for the problem and Sec. II D will solve the model of restricted rotational diffusion in a cone. In Sec. III, the orientational response functions will be expanded in terms of spherical harmonics and solved for in terms of the correlation functions derived in Sec. II D. The general theory applied here is used to describe the TRSHG and TRSFG observables in detail in Sec. III and model calculations and analysis of experimental data are presented in Sec. IV.

A. Electric-field-matter interactions

The TRSHG and TRSFG experiments include the electronic or vibrational excitation of the molecules under study, followed by a time-delayed second SHG probe or SFG probe. The pump laser may be either an infrared laser or a visible laser and the probe may be either SHG or SFG. Combination of the pumping and probing schemes results in four experiments, three of which are likely to provide molecular information. These three experiments are visible-pump-SHG probe, visible-pump-SFG probe, and infrared-pump-SFG probe. The visible laser (with frequency denoted ω_{vis}) is often a near-IR laser with wavelength 800 nm. For performing a SHG probe experiment it is advantageous for this laser to be two-photon resonant with an electronic excited state. This allows for efficient pumping via frequency-doubled laser light and efficient probing via two-photon-resonance enhancement. The IR laser should be resonant with a vibration of interest; typical wavelengths are $3-5\ \mu$m.

Both the pump-SHG probe and pump-SFG probe experiments are fourth-order nonlinear optical experiments, which are described by tensorial nonlinear response functions. Here, the physical origin of the signals will be discussed while in Sec. II B, the tensorial nature will be addressed. For such processes, it is useful to expand the response functions using diagrammatic perturbation theory.[45,46] Within this treatment, the total response function is found to consist of a sum of multiple, independent, double-sided Feynman diagrams. Each diagram represents the contribution of a time correlation function to the measured signal. Formally, each time correlation function, and therefore diagram, is a single term expanded from the nested commutator that results from the perturbation theory treatment.[45] The full response function also includes the complex conjugates of the diagrams shown.

Each double-sided Feynman diagram consists of a series of density matrix elements drawn vertically, one above the previous. The axis of time increases from the bottom to the top of the diagram. Each interaction is separated by a time τ_n as shown along side of Fig. 1(a). The period between the two pump fields and the SHG or SFG probe is referred to as the population period. During the population period, electronic or vibrational relaxation occurs simultaneously with orientational relaxation (the topic of this paper). In between any two density matrix elements, an arrow is drawn indicating an interaction with an electric field. Arrows pointing toward the density matrix elements indicate an absorption process; arrows pointing away from the density matrix elements indicate an emission process. Absorption or emission can occur on either the bra or ket side of the density matrix element. The final signal emission is, by convention, always on the ket side of the diagram. The final signal wave vector is a signed sum of the excitation field wave vectors $\boldsymbol{k}_n$, where each wave vector is added when it corresponds to absorption on the ket side (or emission on the bra side) and subtracted

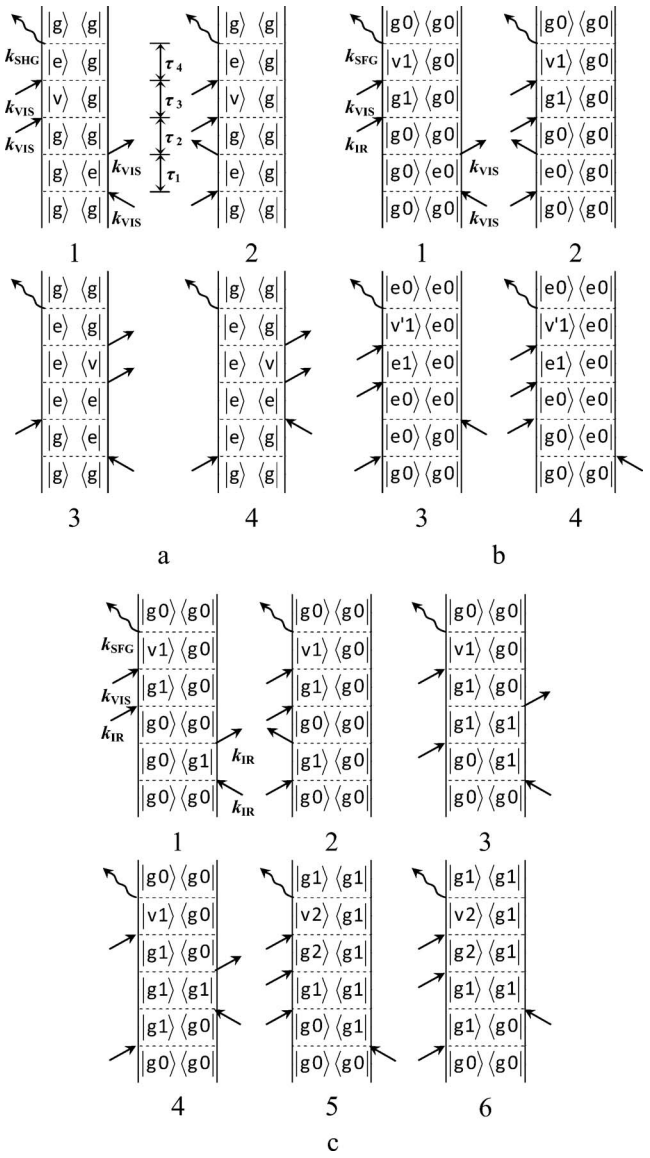

FIG. 1. Double-sided Feynman diagrams for the (a) VIS-pump-SHG, (b) VIS-pump-SFG, and (c) IR-pump-SFG experiments. g, v, and e denote the electronic ground, virtual, and excited states, respectively. 0, 1, and 2 denote the vibrational ground and excited states, respectively. For a discussion of the interpretation of such diagrams, please refer to the text (Sec. II A). The time evolution of the population state formed in the pump field-matter interaction is considered extensively in the text.

when it corresponds to emission on the ket side (or absorption on the bra side). Such wave vector addition (phase matching) permits spatial filtering of different nonlinear signals. The emission frequency is calculated in an identical fashion; only the excitation frequencies ω_n are summed. The sign of the diagram is $(-1)^n$ where n is the number of bra side interactions. The time ordering of the pulses is indicated by the relative vertical position of their corresponding arrows on the diagram. For a more detailed explanation of the underlying theory of the diagrams, we refer the reader to the standard texts.[45,46]

The diagrams for pump-SHG probe and pump-SFG probe (both visible and IR pump) are shown in Fig. 1. Only phase-matched diagrams are included. Generally, the diagrams share a similar structure in that two pump fields bring the system into a population state. The population state is then probed via two electric fields resulting in a coherence which emits the signal to form another population state. In both SFG and SHG experiments the probe process is the result of both a dipole and polarizability interaction. For SFG, the visible wave is scattered inelastically off of the vibrational coherence. For SHG, the two electric fields of the polarizability interaction bring the system into an electronic coherence which radiates via dipole radiation. When the nonresonant interaction is the final interaction (as in SFG) the emitted signal and excitation field are always on the same side of the density matrix element.

Specifically referring to Fig. 1(a), two visible electric fields interact with the bra side of the diagram, creating population in the ground state (g). This population is then excited by two electric fields through a virtual electronic state (v) to create a coherent superposition state between the ground electronic state and the first excited electronic state (e). This excited superposition state then oscillates at the electronic resonance frequency emitting dipole radiation in the phase matched direction, $\boldsymbol{k}_{\mathrm{sig}}=+2\boldsymbol{k}_{\mathrm{vis}}$. The other diagrams in Fig. 1(a) may be interpreted similarly. Including the sign convention discussed above, it is seen that the Feynman paths that proceed through ground and excited electronic population states differ by a negative sign. This indicates that the visible-pump-SHG signal is related to the difference in electronic polarizability upon excitation. For Fig. 1(a), it has been assumed that the system is a two-level electronic system. Other diagrams can be included if it is possible for higher electronic excited states to be probed.

The diagrams for the visible-pump-SFG probe experiment are shown in Fig. 1(b) and can be interpreted in the same manner. In this experiment, the signal not only depends on the change in the polarizability upon electronic excitation but also any changes in vibrational oscillator strength or frequency induced by electronic excitation. The SFG probe step proceeds via a dipole interaction and subsequent Raman interaction which is of opposite time ordering compared to the SHG probe experiment. In Fig. 1(c), the diagrams for the IR pump-SFG probe experiment are shown. Here, the system is assumed to be a three level vibrational system with only virtual electronic states accessible via the visible upconversion laser. The signal depends on ground state bleaching, stimulated emission, and excited state absorption signals. These signals are analogous to those studied by traditional infrared-pump-probe and two-dimensional infrared spectroscopy.[34,47,48]

As the underlying matter-field interactions involve nonresonant polarizability interactions, the symmetry of the molecular polarizability tensor must be known in order to calculate the polarization dependence of the signal. To simplify further calculations, the molecules being probed spectroscopically are assumed to be symmetric tops, which permits the use of a diagonal polarizability tensor of the form

$$\bar{\alpha}=\alpha\begin{pmatrix}1&0&0\\0&1&0\\0&0&1\end{pmatrix}+\beta\begin{pmatrix}-1/3&0&0\\0&-1/3&0\\0&0&2/3\end{pmatrix}, \tag{4}$$

where α and β are the isotropic and anisotropic parts of the polarizability, respectively. This form imposes some restric-

TABLE I. Resonant and nonresonant interactions projected onto the laboratory frame and expressed with spherical harmonics. For the nonresonant interactions, a diagonal polarizability tensor is assumed. $\alpha_\perp=\alpha+2\beta/3$, $\alpha_\parallel=\alpha-\beta/3$ [see Eq. (4)].

Interaction	Projection onto the laboratory frame	Spherical harmonic representation
	Resonant interactions	
$(\hat{\mu}_i\hat{\varepsilon}_Z)$	$\cos\theta_i$	$2(\pi/3)^{1/2}Y_1^0(\Omega_i)$
$(\hat{\mu}_i\hat{\varepsilon}_Y)$	$\sin\theta_i\sin\phi_i$	$i(2\pi/3))^{1/2}(Y_1^{-1}(\Omega_i)+Y_1^1(\Omega_i))$
$(\hat{\mu}_i\hat{\varepsilon}_X)$	$\sin\theta_i\cos\phi_i$	$(2\pi/3)^{1/2}(Y_1^{-1}(\Omega_i)-Y_1^1(\Omega_i))$
$(\hat{\mu}_i\hat{\varepsilon}_{\mathrm{CIRC}})$	$\sin\theta_i$	$[1-(4/3)\pi(Y_1^0(\Omega_i))^2]^{1/2}$
	Nonresonant interactions	
$(\hat{\varepsilon}_Z\bar{\alpha}\hat{\varepsilon}_Z)$	$\alpha_\parallel\cos^2\theta_i+\alpha_\perp\sin^2\theta_i$	$\alpha+(4/3)(\pi/5)\beta Y_2^0(\Omega_i)$
$(\hat{\varepsilon}_Y\bar{\alpha}\hat{\varepsilon}_Y)$	$\alpha_\perp+(\alpha_\parallel-\alpha_\perp)\sin^2\theta_i\sin^2\phi_i$	$\alpha-\beta((2/3)(\pi/5)^{1/2}Y_2^0(\Omega_i)+(2\pi/15)^{1/2}(Y_2^{-2}(\Omega_i)+Y_2^2(\Omega_i)))$
$(\hat{\varepsilon}_X\bar{\alpha}\hat{\varepsilon}_X)$	$\alpha_\perp+(\alpha_\parallel-\alpha_\perp)\sin^2\theta_i\cos^2\phi_i$	$\alpha+\beta(-(2/3)(\pi/5)^{1/2}Y_2^0(\Omega_i)+(2\pi/15)^{1/2}(Y_2^{-2}(\Omega_i)+Y_2^2(\Omega_i)))$
$(\hat{\varepsilon}_Y\bar{\alpha}\hat{\varepsilon}_Y)$	$(\alpha_\parallel-\alpha_\perp)\cos\theta_i\sin\theta_i\sin\phi_i$	$i\beta(2\pi/15)^{1/2}(Y_2^{-1}(\Omega_i)+Y_2^1(\Omega_i))$
$(\hat{\varepsilon}_Z\bar{\alpha}\hat{\varepsilon}_Y)$		
$(\hat{\varepsilon}_X\bar{\alpha}\hat{\varepsilon}_Z)$	$(\alpha_\parallel-\alpha_\perp)\cos\theta_i\sin\theta_i\cos\phi_i$	$\beta(2\pi/15)^{1/2}(Y_2^{-1}(\Omega_i)-Y_2^1(\Omega_i))$
$(\hat{\varepsilon}_Z\bar{\alpha}\hat{\varepsilon}_X)$		
$(\hat{\varepsilon}_X\bar{\alpha}\hat{\varepsilon}_Y)$	$(\alpha_\parallel-\alpha_\perp)\sin\theta_i\sin\phi_i\cos\phi_i$	$i\beta(2\pi/15)^{1/2}(Y_2^{-2}(\Omega_i)-Y_2^2(\Omega_i))$
$(\hat{\varepsilon}_Y\bar{\alpha}\hat{\varepsilon}_X)$		

tion on the model, but it is a sound physical model that can be used for a wide variety of probes at interfaces and surfaces.

Although not denoted in the diagrams, each field can possess its own polarization which affects the signal strength and the orientational properties that are probed during the population period. The projections of the interactions onto the laboratory Cartesian coordinates and their spherical harmonic representations are shown in Table I. In one special case, the pump beam is taken to propagate along the laboratory Z axis and circularly polarized in the XY plane. This polarization scheme was extensively applied in the literature.[19,24,25]

B. The tensorial nonlinear polarization and the material response function

The SHGs and SFGs are nonlinear responses to multiple applied electric fields. In the perturbative limit, the material polarization arising in the nonlinear processes is given by

$$P_\eta=\chi^{(1)}_{\eta\alpha}E_\alpha+\chi^{(2)}_{\eta\beta\alpha}E_\beta E_\alpha+\chi^{(3)}_{\eta\gamma\beta\alpha}E_\gamma E_\beta E_\alpha+\chi^{(4)}_{\eta\delta\gamma\beta\alpha}E_\delta E_\gamma E_\beta E_\alpha+\ldots, \tag{5}$$

where $\chi^{(n)}$ is the nth-order susceptibility. The susceptibility is a tensor function of the frequency and polarization of the fields E_i (denote with Greek subscripts in the general case). In a regular SHG or SFG experiment, only the second term is considered.[10] Not every polarization combination of the interacting fields is allowed. At azimuthally symmetric surfaces and interfaces ($C_{\infty v}$ symmetry), only the following second-order nonlinear susceptibilities are nonzero: $\chi^{(2)}_{ZZZ}, \chi^{(2)}_{ZXX}=\chi^{(2)}_{ZYY}, \chi^{(2)}_{XZX}=\chi^{(2)}_{YZY}, \chi^{(2)}_{XXZ}=\chi^{(2)}_{YYZ}$, where the polarizations are given in the laboratory frame. The material polarization in TRSHG probe and TRSFG probe experiments is equal to the fourth term of the perturbative expansion in Eq. (5). The pump field polarization can be any linear combination of the X, Y, and Z coordinates. A circularly polarized pump beam can also be applied that usually propagates along the Z axis.[19,24,25] Although the dynamics of the molecular system is contained in $\chi^{(n)}$ in the frequency domain, the knowledge of the time-domain material response function $\mathbf{R}^{(n)}$ is more practical for time-resolved experiments. The time-domain material response function is the inverse Fourier-transform of the nonlinear susceptibilities[46,45]

$$R^{(n)}_{\eta\ldots\alpha}(t_n,\ldots,t_1)=\frac{1}{(2\pi)^n}\int_{-\infty}^{\infty}d\omega_n\ldots\int_{-\infty}^{\infty}d\omega_1\chi^{(n)}_{\eta\ldots\alpha}\times\exp(-i(\omega_1+\ldots+\omega_n)t_n)\ldots\times\exp(-i\omega_1t_1). \tag{6}$$

In Eq. (6), $R^{(n)}$ is the $(n+1)$-time correlation function that describes the system for a given time ordering. It is a tensor function that retains the symmetry properties of the nonlinear susceptibility $\chi^{(n)}$. Generally, it is a valid assumption that the orientational motions are decoupled from the vibronic modes of the system, and the time-domain material response function can be separated into contributions from the vibrational and orientational degrees of freedom,

$$R^{(n)}_{\eta\ldots\alpha}(t_n,\ldots,t_1)=R^{(n)}_{\eta\ldots\alpha}(t_n,\ldots,t_1)R_V(t_n,\ldots,t_1), \tag{7}$$

where $R^{(n)}_{\eta\ldots\alpha}(t_n,\ldots,t_1)$ is the orientational response function and $R_V(t_n,\ldots,t_1)$ is the vibrational response function.[49] Only the effect of $R^{(n)}_{\eta\ldots\alpha}(t_n,\ldots,t_1)$ on the nonlinear material polarization will be discussed here.

The pump interactions are taken to be instantaneous. The time-dependences of the emission coherence for the SHG probe case or the vibrational coherence for the SFG case do not influence the orientational relaxation observables during the population period, and will not be considered. Within these conditions, the orientational correlation function can be greatly simplified and expressed as a two-time correlation function,

$$R^{\mathrm{SHG}}_{\eta\delta\gamma\alpha\alpha}(t_1) = \int d\Omega_1 \int d\Omega_0 (\hat{\mu}_1\hat{\varepsilon}_\eta\hat{\varepsilon}_\delta\hat{\alpha}_1\hat{\varepsilon}_\gamma) G(\Omega_1, t_1|\Omega_0)(\hat{\mu}_0\hat{\varepsilon}_\alpha)^2, \tag{8}$$

$$R^{\mathrm{SFG}}_{\eta\delta\gamma\alpha\alpha}(t_1) = \int d\Omega_1 \int d\Omega_0 (\hat{\varepsilon}_\eta\hat{\alpha}_1\hat{\varepsilon}_\delta\hat{\mu}_1\hat{\varepsilon}_\gamma) G(\Omega_1, t_1|\Omega_0)(\hat{\mu}_0\hat{\varepsilon}_\alpha)^2, \tag{9}$$

where $G(\Omega_1, t|\Omega_0)$ is a time propagator or Green's function (see below). A shorthand notation can be introduced to write the above equations in an abbreviated form as

$$R^{\mathrm{SHG}}_{\eta\delta\gamma\alpha\alpha}(t_1) = \langle (\hat{\mu}_\eta\hat{\alpha}_{\delta\gamma})_1(\hat{\mu}_\alpha\hat{\mu}_\alpha)_0\rangle \tag{10}$$

and

$$R^{\mathrm{SFG}}_{\eta\delta\gamma\alpha\alpha}(t_1) = \langle (\hat{\alpha}_{\eta\delta}\hat{\mu}_\gamma)_1(\hat{\mu}_\alpha\hat{\mu}_\alpha)_0\rangle. \tag{11}$$

The simultaneity of the final three interactions imposes additional symmetry conditions on the correlation functions and permits the interchange of certain pulse pairs, similar to the Kleinman symmetry (see Sec. III A).[10]

The physical interpretation of the above equations is intuitive: after the electronic or vibrational excitation with the pump pulse, the population state (see Fig. 1) evolves in time. The time evolution is given by the $G(\Omega_1, t|\Omega_0)$ operator, which is the joint probability of finding the probe at orientation Ω_1 at time t_1, provided it was at orientation Ω_0 at $t=0$. Then, at t_1, the state of orientation is projected onto the probe and signal polarizations. In the general description, the time-evolution operator (the Green's function) depends on the model of reorientation. In the free rotation, for example, it can be expanded as a series of spherical harmonics[32,50]

$$G(\Omega_i, t_i|\Omega_0) = \sum_{n=0}^{\infty}\sum_{m=-n}^{n} c_n^m(t_i) Y_n^{m^*}(\Omega_0) Y_n^m(\Omega_i), \tag{12}$$

where the expansion coefficients are given by

$$c_n^m(t_i) = \exp[-n(n+1)D_{\mathrm{or}}t_i] \tag{13}$$

and the spherical harmonics are defined over the angular coordinates Ω in the laboratory frame (see below). For restricted rotational diffusion within a particular solid angle or cone, the time-evolution operator has a *different form*, and the integration is taken only over the restricted angular volume.

C. Definition of angular variables

As mentioned above, the molecules will be treated as rigid, cylindrically symmetric rods although the formalism can be extended to other shapes. For the nonresonant interactions, the molecules are taken to be symmetric tops, which is consistent with a cylindrical shape. A symmetric top simplifies the results because the polarizability tensor is diagonal. The IR and electronic transition dipoles lie along the symmetry axis of the polarizability of the rod. The procedure can be generalized to any other polarizability tensor symmetry.

The measured correlation functions will be calculated as a two-time correlation function. If the orientation of the molecule is given in the polar coordinates by $\Omega=(\theta,\phi)$, and the interactions are represented with spherical harmonics, the polarization dependent components of the tensorial correlation function will be obtained in the form of dynamic ensemble averages of spherical harmonics: $\langle Y_l^m(\Omega(t))Y_l^m(\Omega(0))\rangle$. After obtaining the correlation functions in this general form, the wobbling-in-a-cone model will be applied to express them as exponential decays.

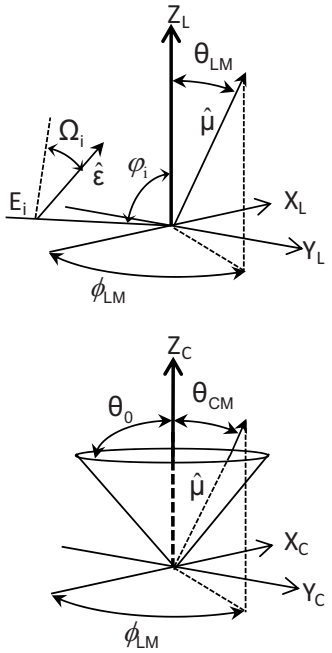

FIG. 2. Angular variables in the laboratory frame (upper) and the conical frame (lower). The sample surface is in the XY plane. The probe and signal beams propagate in the XZ plane incident from the Z_L axis by the angle φ_i and polarized from the vertical by the angle Ω_i. θ_o denotes the cone half-angle and the orientation of a molecule is given by the polar and azimuthal angles $\Omega_{\mathrm{LM}}(t)=(\theta_{\mathrm{LM}}(t),\phi_{\mathrm{LM}}(t))$ and $\Omega_{\mathrm{CM}}(t)=(\theta_{\mathrm{CM}}(t),\phi_{\mathrm{CM}}(t))$ in the laboratory and conical frames, respectively.

Figure 2 illustrates the relevant angular variables for the surface experiments. The excitation and output beams propagate in the XZ plane. Their incident angle is measured from the Z axis and denoted by φ_i. The beams are polarized from the vertical with the angle Ω_i. This gives the projection of the electric field onto the Cartesian axes as

$$\hat{\varepsilon}_i = |\hat{\varepsilon}_i|(\cos\Omega_i\cos\varphi_i\hat{\varepsilon}_Z + \cos\Omega_i\hat{\varepsilon}_Y + \cos\Omega_i\cos\varphi_i\hat{\varepsilon}_X). \tag{14}$$

The orientation of a molecule in the laboratory frame at any time can be given by the polar and the azimuthal angles $\Omega_{\mathrm{LM}}(t)=(\theta_{\mathrm{LM}}(t),\phi_{\mathrm{LM}}(t))$.

It is practical to define a coordinate system that is fixed to the conical volume in which the orientational diffusion of the molecules is restricted. The Z axis of the conical frame is the symmetry axis of the cone, and if it is tilted from the laboratory Z axis by the angle θ_{LC}, the Euler angles that transform the laboratory frame into the conical frame are $(\theta_{\mathrm{LC}},\varphi_{\mathrm{LC}},\chi_{\mathrm{LC}})$. The Euler angles are not functions of the time and can be factored out from the laboratory frame correlation functions.

Within the conical frame, the orientation of the molecule is given by the polar and the azimuthal angles $\Omega_{\mathrm{CM}}(t)$

$=(\theta_{CM}(t),\phi_{CM}(t))$. In the cone model, the polar angle is restricted to $0<\theta_{CM}(t)<\theta_o$, where θ_o denotes the half-cone angle.

Using SFG (or SHG), it is possible to measure the average angle of orientation of a molecule. Within the tilted cone model the average angle can be expressed as

$$\langle\theta\rangle=\frac{\int_{\theta_{LC}-\theta_o}^{\theta_{LC}+\theta_o}\theta\sin\theta d\theta}{\int_{\theta_{LC}-\theta_o}^{\theta_{LC}+\theta_o}\sin\theta d\theta}, \tag{15}$$

which is equivalent to

$$\langle\cos\theta\rangle=\frac{1+\cos\theta_o}{2}, \tag{16}$$

when $\theta_{LC}=0$.[18,51]

D. Orientational correlation functions for restricted rotational diffusion

As mentioned above, the orientational relaxation of the molecules at a surface or interface cannot be described as isotropic diffusion as is the case in bulk liquids. Instead, we adopt the model of wobbling-in-a-cone that has proved to be useful in a numerous of previous problems.[31,42,52–55] To simplify the problem, molecules are assumed to be rigid rods that diffuse freely within a given angular volume, the cone. This model was also suggested by Shen and co-workers[51] for interfacial OH bonds. The orientation of a molecule at a given time can be specified by its polar coordinates within the cone $\Omega_{CM}(t)=(\theta_{CM}(t),\phi_{CM}(t))$.

The diffusion in a cone model was first solved by Warchol and Vaughan.[29] Later Wang and Pecora obtained the $\langle Y_l^m(\Omega(t))Y_l^m(\Omega(0))\rangle$ ($l=1,2$ and $m=0,1,2$) correlation functions within this model.[30]

With conical boundary conditions and with initial condition

$$c(\Omega,0)=\delta(\Omega-\Omega(0))=\delta(\cos\theta-\cos\theta(0))\delta(\phi-\phi(0)), \tag{17}$$

the general solution of the rotational diffusion equation is

$$c(\Omega,t)=\sum_{n=1}^{\infty}\sum_{m=-\infty}^{\infty}\exp(-\nu_n^m(\nu_n^m+1)D_{or}t)Y_{\nu_n^m}^{m^*}(\Omega(0))Y_{\nu_n^m}^m(\Omega(t)), \tag{18}$$

where $c(\Omega,t)$ is the probability density for finding the rod in orientation Ω at time t, D_{or} is the diffusion constant $Y_{\nu_n^m}^m$ denotes the associated spherical harmonics, ν_n^m depends on the cone half-angle and can be *fractional* unlike in the free diffusion model, and the * indicates the complex conjugate of the associated spherical harmonic.[56,57]

The joint probability of finding a rod with orientation $\Omega(0)$ in solid angle $d\Omega(0)$ at time $t=0$ and orientation $\Omega(t)$ in solid angle $d\Omega(t)$ at time t is then,

$$G_s(\Omega(t),t|\Omega(0),0)=\frac{1}{2\pi(1-\cos\theta_o)}\sum_{n=1}^{\infty}\sum_{m=-\infty}^{\infty}\exp(-\nu_n^m(\nu_n^m+1)D_{or}t)\times Y_{\nu_n^m}^{m^*}(\Omega(0))Y_{\nu_n^m}^m(\Omega(t)), \tag{19}$$

where the Green's function satisfies the normalization condition

$$\int\int G_s(\Omega(t),t|\Omega(0),0)d\Omega(t)d\Omega(0)=1. \tag{20}$$

The angular integrals are taken only over the conical volume accessible to the molecule through diffusion.

These results lead to the orientational correlation functions that can be written as ensemble averages of spherical harmonics

$$\langle Y_l^{m^*}(\Omega(t))Y_{l'}^{m'}(\Omega(0))\rangle=\int d\Omega(0)\int d\Omega(t)Y_l^{m^*}(\Omega(t))G_s(\Omega(t),t|\Omega(0))Y_{l'}^{m'}(\Omega(0)). \tag{21}$$

In general, the ensemble averages have the following form:

$$\langle Y_l^{m^*}(\Omega(t))Y_{l'}^{m'}(\Omega(0))\rangle=\frac{\delta_{mm'}}{4\pi}\sqrt{\frac{(2l+1)(2l'+1)(l-m)!(l'-m)!}{(l+m)!(l'+m)!}}\times\sum_{n=1}^{\infty}C_n^m\exp(-\nu_n^m(\nu_n^m+1)D_{or}t) \tag{22}$$

and

$$\langle Y_l^{m^*}(\Omega(t))Y_{l'}^{m'}(\Omega(0))\rangle=\langle Y_l^{-m^*}(\Omega(t))Y_{l'}^{-m'}(\Omega(0))\rangle, \tag{23}$$

i.e., the orientational correlation function is an infinite sum of exponential decays.

The C_n^m coefficients are calculated as

$$C_n^m=\frac{1}{H_n^m(1-\cos\theta_o)}\int_0^{\theta_o}d\theta\sin\theta P_l^m(\cos\theta)P_{\nu_n^m}^m(\cos\theta)\times\int_0^{\theta_o}d\theta'\sin\theta' P_{l'}^{m'}(\cos\theta')P_{\nu_n^{m'}}^{m'}(\cos\theta'), \tag{24}$$

where

$$H_n^m=\int_0^{\theta_o}d\theta\sin\theta P_{\nu_n^m}^m(\cos\theta)P_{\nu_n^m}^m(\cos\theta'). \tag{25}$$

Using the integrals from Eqs. (24) and (25) in Eq. (22), the orientational correlation functions for any l and m can be calculated. Unfortunately, most of these integrals can only be calculated numerically. However, for each l and m, it is shown in Appendix A that the summation can be truncated after the first decaying exponential term because the combination of all of the other terms is negligible for cone half-angles that will be encountered in the vast majority of systems. In addition, Appendix A also shows that for the SHG

and SFG experimental observables, the necessary coefficients C_n^m can be obtained analytically in terms of the cone half-angle. Furthermore, while the ν_n^m coefficients can only be calculated numerically, they can be well approximated by analytical formulae for $\theta_o < 170°$, which is a half-angle that is larger than expected for most surface and interfacial systems. The net result is that Eq. (22) reduces to a tractable expression that can be accurately calculated analytically. The necessary terms are either a single exponential or a constant plus a single exponential.

We will also need to calculate both $\langle Y_l^{m^*}(\Omega(t))\rangle$ and $\langle Y_l^m(\Omega(0))\rangle$. The average value of these single spherical harmonics is

$$\langle Y_l^{m^*}(\Omega(t))\rangle = \langle Y_l^m(\Omega(0))\rangle = \frac{\delta_{m0}}{1-\cos\theta_o}\sqrt{\frac{2l+1}{4\pi}}\int_0^{\theta_o} P_l(\cos\theta)\sin\theta d\theta, \tag{26}$$

where P_l is the lth order Legendre polynomial.[33,58]

For the isotropic case, Wang and Pecora[30] calculated the $\langle Y_l^{m^*}(\Omega(t))Y_l^m(\Omega(0))\rangle$ $(l=1,2)$ correlation functions. However, for TRSHG and TRSFG experiments, different correlation functions are needed and are derived below in a manner similar to the $l=1,2$ cases. In the end, the necessary correlation functions are obtained as exponential decays.

Armed with expressions for the time correlation functions of spherical harmonics, it will now be possible to calculate the exact orientational response given the experimental polarization conditions for a TRSHG or TRSFG experiment. In Sec. III, we will first demonstrate the proper expansion of the orientational response into spherical harmonics and then plug in the results from the above section.

III. RESULTS FOR TRSHG AND TRSFG EXPERIMENTS

A. The orientational correlation functions in the laboratory frame

First the orientational correlation functions $R^{\mathrm{SHG}}_{\eta\delta\gamma\alpha\alpha}$ and $R^{\mathrm{SFG}}_{\eta\delta\gamma\alpha\alpha}$ will be calculated in the laboratory frame. It requires the evaluation of the integrals in Eqs. (8) and (9). The time-evolution operator $G(\Omega_1,t|\Omega_0)$ is not evaluated in this step and the orientational correlation functions will be obtained in a general form as a sum of the dynamic ensemble averages of spherical harmonics $\langle Y_l^{m^*}(\Omega(t))Y_l^m(\Omega(0))\rangle$.

The electric-field-dipole and electric-field-polarizability interactions are transformed into the laboratory frame and represented with spherical harmonics in Table I. When the fields are temporally and spatially overlapped, the spherical harmonic representations of the interactions can always be written as the sums of a constant and spherical harmonics of the order from one to three. The purely algebraic transformations of the spherical harmonic representations are given in detail in Appendix B for completeness.

Symmetry relations can reduce the number of correlation functions that need to be calculated. The simultaneity of the final three interactions [see Eq. (4), Table I, and Fig. 1] permits the interchange of certain pulse pairs, and one can obtain the following symmetry relationships (the electric field is either linearly polarized along the Cartesian axes X, Y, and Z or circularly polarized in the XY plane denoted by C in the subscript):

$$R^{\mathrm{SHG}}_{ZZZZZ} = R^{\mathrm{SFG}}_{ZZZZZ}, R^{\mathrm{SHG}}_{ZZZYY} = R^{\mathrm{SHG}}_{ZZZXX} = R^{\mathrm{SFG}}_{ZZZYY} = R^{\mathrm{SFG}}_{ZZZXX}, \tag{27}$$

$$R^{\mathrm{SHG}}_{ZYYZZ} = R^{\mathrm{SFG}}_{YYZZZ}, R^{\mathrm{SHG}}_{ZYYYY} = R^{\mathrm{SFG}}_{YYZYY}, R^{\mathrm{SHG}}_{ZYYXX} = R^{\mathrm{SFG}}_{YYZXX}, \tag{28}$$

$$R^{\mathrm{SHG}}_{ZXXZZ} = R^{\mathrm{SFG}}_{XXZZZ}, R^{\mathrm{SHG}}_{ZXXYY} = R^{\mathrm{SFG}}_{XXZYY}, R^{\mathrm{SHG}}_{ZXXXX} = R^{\mathrm{SFG}}_{XXZXX}, \tag{29}$$

$$R^{\mathrm{SHG}}_{YYZZZ} = R^{\mathrm{SHG}}_{YZYZZ} = R^{\mathrm{SFG}}_{YZYZZ} = R^{\mathrm{SFG}}_{ZYYZZ}, R^{\mathrm{SHG}}_{YYZYY} = R^{\mathrm{SHG}}_{YZYYY} = R^{\mathrm{SFG}}_{YZYYY} = R^{\mathrm{SFG}}_{ZYYYY}, \tag{30}$$

$$R^{\mathrm{SHG}}_{YYZXX} = R^{\mathrm{SHG}}_{YZYXX} = R^{\mathrm{SFG}}_{YZYXX} = R^{\mathrm{SFG}}_{ZYYXX},$$

$$R^{\mathrm{SHG}}_{XXZZZ} = R^{\mathrm{SHG}}_{XZXZZ} = R^{\mathrm{SFG}}_{XZXZZ} = R^{\mathrm{SFG}}_{ZXXZZ}, R^{\mathrm{SHG}}_{XXZYY} = R^{\mathrm{SHG}}_{XZXYY} = R^{\mathrm{SFG}}_{XZXYY} = R^{\mathrm{SFG}}_{ZXXYY} \tag{31}$$

$$R^{\mathrm{SHG}}_{XXZXX} = R^{\mathrm{SHG}}_{XZXXX} = R^{\mathrm{SFG}}_{XZXXX} = R^{\mathrm{SFG}}_{ZXXXX},$$

$$R^{\mathrm{SHG}}_{ZZZCC} = R^{\mathrm{SFG}}_{ZZZCC}, R^{\mathrm{SHG}}_{ZYYCC} = R^{\mathrm{SFG}}_{YYZCC}, R^{\mathrm{SHG}}_{ZXXCC} = R^{\mathrm{SFG}}_{XXZCC}, \tag{32}$$

$$R^{\mathrm{SHG}}_{YYZCC} = R^{\mathrm{SHG}}_{YZYCC} = R^{\mathrm{SFG}}_{YZYCC} = R^{\mathrm{SFG}}_{ZYYCC}, R^{\mathrm{SHG}}_{XXZCC} = R^{\mathrm{SHG}}_{XZXCC} = R^{\mathrm{SFG}}_{XZXCC} = R^{\mathrm{SFG}}_{ZXXCC}. \tag{33}$$

It is sufficient to calculate the orientational correlation functions with the SHG time ordering. The correlation functions with the SFG time ordering can be obtained by using the above symmetry relations. At the azimuthally symmetric ($C_{\infty v}$ symmetry) interfaces, the number of the unique orientational correlation functions is further reduced

$$R^{\mathrm{SHG}}_{ZZZYY} = R^{\mathrm{SHG}}_{ZZZXX}, \tag{34}$$

$$R^{\mathrm{SHG}}_{ZYYZZ} = R^{\mathrm{SHG}}_{ZXXZZ}, R^{\mathrm{SHG}}_{ZYYYY} = R^{\mathrm{SHG}}_{ZXXXX}, R^{\mathrm{SHG}}_{ZYYZZ} = R^{\mathrm{SHG}}_{ZXXZZ}, R^{\mathrm{SHG}}_{ZYYCC} = R^{\mathrm{SHG}}_{ZXXCC}, \tag{35}$$

$$R^{\mathrm{SHG}}_{ZYYYY} = R^{\mathrm{SHG}}_{ZXXXX}, R^{\mathrm{SHG}}_{ZYYXX} = R^{\mathrm{SHG}}_{ZXXYY}, \tag{36}$$

$$R^{\mathrm{SHG}}_{YYZZZ} = R^{\mathrm{SHG}}_{YZYZZ} = R^{\mathrm{SHG}}_{XZXZZ} = R^{\mathrm{SHG}}_{XXZZZ}, R^{\mathrm{SHG}}_{YYZCC} = R^{\mathrm{SHG}}_{YZYCC} = R^{\mathrm{SHG}}_{XZXCC} = R^{\mathrm{SHG}}_{XXZCC}, \tag{37}$$

$$R^{\mathrm{SHG}}_{YYZYY} = R^{\mathrm{SHG}}_{YZYYY} = R^{\mathrm{SHG}}_{XZXXX} = R^{\mathrm{SHG}}_{XXZXX}, R^{\mathrm{SHG}}_{YYZXX} = R^{\mathrm{SHG}}_{YZYXX} = R^{\mathrm{SHG}}_{XZXYY} = R^{\mathrm{SHG}}_{XXZYY}. \tag{38}$$

Therefore, the unique orientational correlation functions that need to be calculated are

R^{SHG}_{ZZZZZ}, R^{SHG}_{ZZZYY}, R^{SHG}_{ZYYZZ}, R^{SHG}_{ZYYYY}, R^{SHG}_{ZYYXX}, R^{SHG}_{YYZZZ}, R^{SHG}_{YYZYY}, R^{SHG}_{YYZXX}, R^{SHG}_{ZZZCC}, R^{SHG}_{ZYYCC},

and

R^{SHG}_{YYZCC}.

TABLE II. The orientational correlation functions for tensor elements of the fourth-order polarization for the TRSHG experiments calculated from Eq. (8). For simplicity, the following notation is used: $\langle Y_l^m Y_2^m\rangle = \langle Y_l^{m^*}(\Omega_{\mathrm{lab}}(t)) G_S(\Omega_{\mathrm{lab}}(t),t;\Omega_{\mathrm{lab}}(0),0) Y_2^m(\Omega_{\mathrm{lab}}(0))\rangle$. α and β are the isotropic and anisotropic part of the polarizability tensor [see Eq. (4)].

R_{ZZZCC}	$\frac{4}{4725}((15\alpha+4\beta)(-14\sqrt{15}\pi\langle Y_1^0Y_2^0\rangle+35\sqrt{3\pi}\langle Y_1^0\rangle)-9\sqrt{7}\beta(4\sqrt{5}\pi\langle Y_3^0Y_2^0\rangle-10\sqrt{\pi}\langle Y_3^0\rangle))$
R_{ZYYCC}	$\frac{4}{4725}((15\alpha-2\beta)(-14\sqrt{15}\pi\langle Y_1^0Y_2^0\rangle+35\sqrt{3\pi}\langle Y_1^0\rangle)+9\sqrt{7}\beta(2\sqrt{5}\pi\langle Y_3^0Y_2^0\rangle-5\sqrt{\pi}\langle Y_3^0\rangle))$
R_{YYZCC}	$\frac{4}{1575}\beta(-14\sqrt{15}\pi\langle Y_1^0Y_2^0\rangle+35\sqrt{3\pi}\langle Y_1^0\rangle+6\sqrt{35}\pi\langle Y_3^0Y_2^0\rangle-15\sqrt{7\pi}\langle Y_3^0\rangle)$
R_{ZZZZZ}	$\frac{2}{4725}((15\alpha+4\beta)(28\sqrt{15}\pi\langle Y_1^0Y_2^0\rangle+35\sqrt{3\pi}\langle Y_1^0\rangle)+9\sqrt{7}\beta(8\sqrt{5}\pi\langle Y_3^0Y_2^0\rangle+10\sqrt{\pi}\langle Y_3^0\rangle))$
R_{ZZZYY}	$\frac{2}{4725}((15\alpha+4\beta)(-14\sqrt{15}\pi\langle Y_1^0Y_2^0\rangle+35\sqrt{3\pi}\langle Y_1^0\rangle)-9\sqrt{7}\beta(4\sqrt{5}\pi\langle Y_3^0Y_2^0\rangle-10\sqrt{\pi}\langle Y_3^0\rangle))$
R_{ZYYZZ}	$\frac{2}{4725}((15\alpha-2\beta)(28\sqrt{15}\pi\langle Y_1^0Y_2^0\rangle+35\sqrt{3\pi}\langle Y_1^0\rangle)-9\sqrt{7}\beta(4\sqrt{5}\pi\langle Y_3^0Y_2^0\rangle+5\sqrt{\pi}\langle Y_3^0\rangle))$
R_{ZYYYY}	$\frac{2}{4725}((15\alpha-2\beta)(-14\sqrt{15}\pi\langle Y_1^0Y_2^0\rangle+35\sqrt{3\pi}\langle Y_1^0\rangle)+9\sqrt{7}\beta(2\sqrt{5}\pi\langle Y_3^0Y_2^0\rangle+10\pi\langle Y_3^2Y_2^2\rangle-5\sqrt{\pi}\langle Y_3^0\rangle))$
R_{ZYYXX}	$\frac{2}{4725}((15\alpha-2\beta)(-14\sqrt{15}\pi\langle Y_1^0Y_2^0\rangle+35\sqrt{3\pi}\pi Y_1^0)+9\sqrt{7}\beta(2\sqrt{5}\pi\langle Y_3^0Y_2^0\rangle-10\pi\langle Y_3^2Y_2^2\rangle-5\sqrt{\pi}\langle Y_3^0\rangle))$
R_{YYZZZ}	$\frac{2}{1575}\beta(28\sqrt{15}\pi\langle Y_1^0Y_2^0\rangle+35\sqrt{3\pi}\langle Y_1^0\rangle-12\sqrt{35}\pi\langle Y_3^0Y_2^0\rangle-15\sqrt{7\pi}\langle Y_3^0\rangle)$
R_{YYZYY}	$\frac{2}{1575}\beta(-14\sqrt{15}\pi\langle Y_1^0Y_2^0\rangle+35\sqrt{3\pi}\langle Y_1^0\rangle+6\sqrt{35}\pi\langle Y_3^0Y_2^0\rangle+30\sqrt{7}\pi\langle Y_3^2Y_2^2\rangle-15\sqrt{7\pi}\langle Y_3^0\rangle)$
R_{YYZXX}	$\frac{2}{1575}\beta(-14\sqrt{15}\pi\langle Y_1^0Y_2^0\rangle+35\sqrt{3\pi}\langle Y_1^0\rangle+6\sqrt{35}\pi\langle Y_3^0Y_2^0\rangle-30\sqrt{7}\pi\langle Y_3^2Y_2^2\rangle-15\sqrt{7\pi}\langle Y_3^0\rangle)$

Now, taking the spherical harmonic representations of the field-matter interactions listed in Table I, the orientational correlation functions can be calculated. The detailed derivation is given here for the R_{ZZZZZ}^{SHG} tensor element only. For the other tensor elements, the derivations are similar and the results are listed in Table II.

Using the shorthand notation introduced in Eqs. (10) and (11),

$$R_{ZZZZZ}^{\mathrm{SHG}}(t_1)=\langle(\hat{\mu}_Z\hat{\alpha}_{ZZ})_1(\hat{\mu}_Z\hat{\mu}_Z)_0\rangle. \tag{39}$$

Substituting the spherical harmonic representations of the interactions from Table I and Appendix B, one can obtain

$$R_{ZZZZZ}^{\mathrm{SHG}}(t_1)=\left\langle\left(\frac{2}{15}\sqrt{\frac{\pi}{3}}(15\alpha+4\beta)Y_1^0(\Omega(t_1))+\frac{4}{5}\sqrt{\frac{\pi}{7}}Y_3^0(\Omega(t_1))\right)\left(\frac{1}{3}+\frac{4}{3}\sqrt{\frac{\pi}{5}}Y_2^0(\Omega(0))\right)\right\rangle, \tag{40}$$

which yields

$$\frac{2}{4725}((15\alpha+4\beta)(28\sqrt{15}\pi\langle Y_1^0Y_2^0\rangle+35\sqrt{3\pi}\langle Y_1^0\rangle)+9\sqrt{7}\beta(8\sqrt{5}\pi\langle Y_3^0Y_2^0\rangle+10\sqrt{\pi}\langle Y_3^0\rangle)), \tag{41}$$

where the following notation is used:

$$\langle Y_l^m Y_2^m\rangle=\langle Y_l^{m^*}(\Omega_{\mathrm{lab}}(t))G_S(\Omega_{\mathrm{lab}}(t),t;\Omega_{\mathrm{lab}}(0),0)Y_2^m(\Omega_{\mathrm{lab}}(0))\rangle. \tag{42}$$

The averaging is over the polar and azimuthal angles at time t_1 and $t=0$.

Without applying any orientational diffusion model, the correlation functions are listed in Table II. One can see that the $C_1(t)$ and $C_2(t)$ correlation functions do not appear in the equations. Instead, the

$$\langle Y_l^m Y_2^m\rangle=\int d\Omega(0)\int d\Omega(t)Y_l^{m^*}(\Omega(t))G_s(\Omega(t),t|\Omega(0))Y_2^m(\Omega(0)) \quad (l=1,3;\ m=0,2) \tag{43}$$

correlation functions are measured in the TRSHG and TRSFG experiments. The integrals are performed only over the volume in which the orientational diffusion occurs. The time-evolution operator $G_s(\Omega(t),t|\Omega(0))$ depends on the model of the orientation relaxation and the potential within the volume of diffusion. In certain cases, the operator can be represented by spherical harmonics, which permits the derivation of analytical forms of the correlation functions. If the time-evolution operator cannot be represented in such a way, the correlation functions can be evaluated numerically.

TABLE III. Rotating correlation functions into the tilted cone frame. The symmetry axis of the cone is tilted from the surface normal by the angle θ_{LC}, which does not evolve in time. The relationship between the correlation functions in different frames are given by the addition theorem of spherical harmonics in Eq. (44). $d^i_{j,k}$ denotes the small Wigner d-matrix (see Sec. IV B).

$$\langle \mathbf{Y}_1^0 \mathbf{Y}_2^0 \rangle = \sum_{j=-1}^{1} \langle Y_1^{j^*}(\phi_{CM}(t),\theta_{CM}(t)) Y_2^j(\phi_{CM}(0),\theta_{CM}(0))\rangle d^1_{0j}(\theta_{LC})(-1)^{0-j} d^2_{0(-j)}(\theta_{LC})$$

$$\langle \mathbf{Y}_3^0 \mathbf{Y}_2^0 \rangle = \sum_{j=-2}^{2} \langle Y_3^{j^*}(\phi_{CM}(t),\theta_{CM}(t)) Y_2^j(\phi_{CM}(0),\theta_{CM}(0))\rangle d^3_{0j}(\theta_{LC})(-1)^{0-j} d^2_{0(-j)}(\theta_{LC})$$

$$\langle \mathbf{Y}_3^2 \mathbf{Y}_2^2 \rangle = \sum_{j=-2}^{2} \langle Y_3^{j^*}(\phi_{CM}(t),\theta_{CM}(t)) Y_2^j(\phi_{CM}(0),\theta_{CM}(0))\rangle d^3_{2j}(\theta_{LC})(-1)^{2-j} d^2_{(-2)(-j)}(\theta_{LC})$$

$$\langle \mathbf{Y}_1^0 \rangle = \langle Y_1^0(\phi_{CM}(t),\theta_{CM}(t))\rangle d^1_{00}(\theta_{LC})$$

$$\langle \mathbf{Y}_3^0 \rangle = \langle Y_3^0(\phi_{CM}(t),\theta_{CM}(t))\rangle d^3_{00}(\theta_{LC})$$

B. The $\langle Y_l^m Y_2^m \rangle$ correlation functions in a tilted restricted cone

In Sec. III A, the spherical harmonic correlation functions for a restricted cone model were found. However, to properly represent any molecular orientation at the interface, it is necessary to allow for the cone to be tilted with respect to the surface normal. Here we incorporate this "tilted" frame of reference into the model.

In an *empty cone* whose symmetry axis is the surface normal, the polar coordinates of the molecules within the laboratory (LM) are equal to the coordinates in the cone (CM) frame, i.e., $\Omega_{LM}(t)=\Omega_{CM}(t)$. If the symmetry axis of the cone is *tilted* from the surface normal, the correlation function written in the laboratory frame has to be transformed into the conical frame. This case corresponds to a molecule which reorients within the polar angle interval $[\theta_a, \theta_b]$.

According to the addition theorem of spherical harmonics,[58]

$$Y_l^m(\theta_{LM}(\Omega(t)),\phi_{LM}(\Omega(t))) = \sum_{m'} D^l_{m'm}(\phi_{LC},\theta_{LC},\chi_{LC}) Y_l^{m'}(\theta_{CM}(\Omega(t)),\phi_{CM}(\Omega(t))), \tag{44}$$

where (θ_{LM},ϕ_{LM}) are the polar coordinates of the molecule in the laboratory frame, $(\phi_{LC},\theta_{LC},\chi_{LC})$ are the Euler angles that transform the laboratory frame into the conical frame, and (θ_{CM},ϕ_{CM}) are the polar coordinates of the molecule in the conical frame. $D^l_{m'm}$ denotes the lth order Wigner D matrix.

The Euler angles that connect the laboratory frame with the conical frame are constant, while the polar angles in the conical frame evolve in time. Because the interface and the cone are taken to have a $C_{\infty v}$ symmetry, $\chi_{LC}=0$. Every ϕ_{LC} angle is equally probable; therefore, one can average over the azimuthal angles, and only the tilt angle from the surface normal matters.

Using the orthogonality properties of the ensemble averages of spherical harmonics

$$\langle Y_l^m \rangle = \delta_{m0} \langle Y_l^0 \rangle \tag{45}$$

and

$$\langle Y_l^m Y_{l'}^{m'} \rangle = \delta_{mm'} \langle Y_l^m Y_{l'}^m \rangle, \tag{46}$$

the correlation functions derived in the laboratory frame can be transformed into the conical frame. The laboratory frame correlation functions expressed in the conical frame are listed in Table III.

To illustrate how to transform the correlation functions from the laboratory frame to the conical frame, we examine the R^{SHG}_{ZZZZZ} tensor element derived above. According to Eq. (41), it consists of the $\langle Y_l^0 Y_2^0 \rangle$ $(l=1,3)$ correlation functions and the $\langle Y_l^0 \rangle$ ensemble averages, which can be transformed into the tilted frame individually by using the equations listed in Table III. The Wigner small d matrices can be found in handbooks[58] and the correlation functions in the rotated frame are the following:

$$\langle Y_1^0 Y_2^0 \rangle_L = \sqrt{3}\langle Y_1^1 Y_2^1 \rangle_C \sin^2\theta_{LC}\cos\theta_{LC} + \tfrac{1}{2}\langle Y_1^0 Y_2^0 \rangle_C \cos\theta_{LC}(3\cos^2\theta_{LC}-1), \tag{47}$$

$$\langle Y_3^0 Y_2^0 \rangle_L = \frac{3\sqrt{5}}{4}\langle Y_3^2 Y_2^2 \rangle_C \cos\theta_{LC}\sin^4\theta_{LC} + \frac{3}{4\sqrt{2}}\langle Y_3^1 Y_2^1 \rangle_C \times (3+5\cos(2\theta_{LC}))\cos\theta_{LC}\sin^2\theta_{LC} + \frac{1}{16}\langle Y_3^0 Y_2^0 \rangle_C (3\cos\theta_{LC}+5\cos(3\theta_{LC})) \times (3\cos^2\theta_{LC}-1), \tag{48}$$

where the subscript C denotes an ensemble average in the conical frame.

It can be seen that when $\theta_{LC}=0$, the $\langle Y_l^m Y_2^m \rangle$ $(m=1,2)$ correlation functions vanish in the sums and the correlation functions expressed in the laboratory frame and in the conical frame are identical.

The ensemble averages are obtained as

$$\langle Y_1^0 \rangle_L = \langle Y_1^0 \rangle_C \cos\theta_{LC}, \tag{49}$$

and

$$\langle Y_3^0 \rangle_L = \tfrac{1}{8}\langle Y_3^0 \rangle_C (3\cos\theta_{LC}+5\cos(3\theta_{LC})). \tag{50}$$

Substituting these expressions into Eq. (41), one can get the R^{SHG}_{ZZZZZ} tensor element for the tilted cone case as

TABLE IV. Correlation functions in the conical frame. For transforming the correlation functions from the conical frame into the laboratory frame, see Table III.

$$\langle Y_1^0 Y_2^0\rangle = \frac{\sqrt{15}}{4\pi}\left(\frac{1}{4}\cos\theta_o(1+\cos\theta_o)^2 + \frac{1}{4}\sin^2\left(\frac{\theta_o}{2}\right)\sin^2\theta_o e^{-\nu_2^0(\nu_2^0+1)D_{or}t}\right)$$

$$\langle Y_1^{\pm1} Y_2^{\pm1}\rangle = \frac{3\sqrt{5}}{32\pi}\frac{\sin^4(\theta_o)}{1-\cos(\theta_o)}e^{-\nu_1^1(\nu_1^1+1)D_{or}t}$$

$$\langle Y_3^0 Y_2^0\rangle = \frac{\sqrt{35}}{4\pi}\left(\frac{1}{16}\cos\theta_o(1+\cos\theta_o)^2(5\cos^2\theta_o-1) + \frac{1}{4}\cos^2\left(\frac{\theta_o}{2}\right)\sin^4\left(\frac{\theta_o}{2}\right)(9+10\cos\theta_o+5\cos 2\theta_o)e^{-\nu_2^0(\nu_2^0+1)D_{or}t}\right)$$

$$\langle Y_3^{\pm1} Y_2^{\pm1}\rangle = \frac{\sqrt{35}}{64\pi\sqrt{2}}\left(\frac{(7+5\cos(2\theta_o))\sin^4(\theta_o)}{1-\cos(\theta_o)}\right)e^{-\nu_1^1(\nu_1^1+1)D_{or}t}$$

$$\langle Y_3^{\pm2} Y_2^{\pm2}\rangle = \frac{5\sqrt{7}\sin^6\theta_o}{64\pi(1-\cos\theta_o)}e^{-\nu_1^2(\nu_1^2+1)D_{or}t}$$

$$\langle Y_1^0\rangle = \frac{1}{4}\sqrt{\frac{3}{\pi}}(1+\cos\theta_o)$$

$$\langle Y_3^0\rangle = \frac{1}{16}\sqrt{\frac{7}{\pi}}\cos^2\left(\frac{\theta_o}{2}\right)(3+5\cos(2\theta_o))$$

$$\begin{aligned}R_{ZZZZZ}^{\mathrm{SHG}} = {} & \frac{2}{675}(15\alpha+4\beta)\cos\theta_{LC}(\sqrt{5}\pi\langle Y_1^0 Y_2^0\rangle_C \\ & \times(6+\sqrt{3}+3(\sqrt{3}-2)\cos(2\theta_{LC}))) + \frac{45}{4}\beta\sqrt{7\pi}\langle Y_3^0\rangle_C \\ & \times(3\cos\theta_{LC}+5\cos(3\theta_{LC})) + \frac{9}{2}\sqrt{7}\beta\pi(\sqrt{5}\langle Y_3^0 Y_2^0\rangle_C \\ & \times(3\cos^2(\theta_{LC})-1)(3\cos\theta_{LC}+5\cos(3\theta_{LC}))) \\ & + \frac{9}{2}\sqrt{7}\beta\pi(6\cos\theta_{LC}\sin^2\theta_{LC}(\sqrt{10}\langle Y_1^1 Y_2^1\rangle_C \\ & \times(3+5\cos(2\theta_{LC})) + 10\langle Y_3^2 Y_2^2\rangle_C\sin^2\theta_{LC})). \end{aligned} \quad (51)$$

C. The correlation functions as exponential decays

Within the conical frame, the dynamic ensemble averages $\langle Y_l^m Y_2^m\rangle$ ($l=1,3$, $m=0,1,2$) have to be calculated to describe the orientational relaxation of the molecules. Wang and Pecora[30] solved the $\langle Y_l^m Y_l^m\rangle$ ($l=1,2$, $m=0,1,2$) orientational correlation functions for restricted diffusion and we follow their procedure to obtain the correlation functions to describe the TRSHG and TRSFG experiments. The details of the mathematics are given in Appendix A and here we show only the resulting equations. We used the model of restricted diffusion in a conical volume as outlined in the Sec. II D (see above). According to Eq. (23), it is sufficient to solve the problem for positive m values only, and the correlation functions can be written as an infinite sum of exponential decays. The coefficients of the exponentials can be calculated numerically and it is shown in Appendix B that the sums can always be truncated after the first decaying exponential term.

Table IV shows the results. It can be seen that the correlation functions can be written in the following general form:

$$\langle Y_l^{0^*}(\Omega(t))Y_2^0(\Omega(0))\rangle = A(\theta_o) + B(\theta_o)\exp(-\nu_2^0(\nu_2^0+1)D_{or}t), \quad (l=1,3) \quad (52)$$

and

$$\langle Y_l^{m^*}(\Omega(t))Y_2^m(\Omega(0))\rangle = A(\theta_o)\exp(-\nu_1^m(\nu_1^m+1)D_{or}t), \quad (l=1,3 \text{ and } m\neq 0). \quad (53)$$

It is important to point out that the ν_2^0 and ν_1^m constants depend on the cone half-angle θ_o. While they can only be calculated exactly numerically, for a very wide range of cone half-angles $\theta_o<170°$, they can be very well approximated by the following formulae:[31,38,56,57]

$$\nu_2^0 = \nu_1^2 = 10^{0.496}\theta_o^{-1.122} \quad (54)$$

and

$$\nu_1^1 = 10^{0.237}\theta_o^{-1.122}, \quad (55)$$

where θ_o is in radian. The ν_1^1 coefficient appears only in the tilted cone cases. When the tilt of the cone is not significant, the correlation functions in the conical frame are given as a constant plus a single exponential decay that depend on the half-cone angle. The offset in the tilted case is also nonzero and depends on the ensemble averages of certain spherical harmonics (see Table III).

At this point, we have derived the correlation functions for the restricted diffusion in a cone and the nonzero orientational correlation functions in the laboratory frame. Using the optical beam geometry, the observed pump-SHG probe and pump-SFG probe orientational correlation functions can be constructed from the equations that were derived.

To summarize, to calculate the time correlation functions, one projects the excitation and signal beams onto Cartesian coordinates in the laboratory frame (Table V) and the laboratory frame correlation functions onto the tilted conical frame (Table III). Then, the polarization selective orientational correlation functions in the laboratory frame can be

TABLE V. Polarization dependence of the TRSHG and TRSFG experiments. The beams are incident on the sample surface at the angle ϕ from normal and polarized at Ω from the vertical

$$
\begin{aligned}
\boldsymbol{P}^{(4)} = {} & R_{ZZZZZ} \cos\Omega_{\mathrm{SHG}} \cos^2\Omega_{\mathrm{VIS}} \cos^2\Omega_{\mathrm{pump}} \sin\varphi_{\mathrm{SHG}} \sin^2\varphi_{\mathrm{VIS}} \sin^2\varphi_{\mathrm{pump}} \\
& + R_{ZZZYY} \cos\Omega_{\mathrm{SHG}} \cos^2\Omega_{\mathrm{VIS}} \sin^2\Omega_{\mathrm{pump}} \sin\varphi_{\mathrm{SHG}} \sin^2\varphi_{\mathrm{VIS}} \\
& + R_{ZZZXX} \cos\Omega_{\mathrm{SHG}} \cos^2\Omega_{\mathrm{VIS}} \cos^2\Omega_{\mathrm{pump}} \sin\varphi_{\mathrm{SHG}} \sin^2\varphi_{\mathrm{VIS}} \cos^2\varphi_{\mathrm{pump}} \\
& + R_{ZYYZZ} \cos\Omega_{\mathrm{SHG}} \sin^2\Omega_{\mathrm{VIS}} \cos^2\Omega_{\mathrm{pump}} \sin\varphi_{\mathrm{SHG}} \sin^2\varphi_{\mathrm{pump}} \\
& + R_{ZYYYY} \cos\Omega_{\mathrm{SHG}} \sin^2\Omega_{\mathrm{VIS}} \sin^2\Omega_{\mathrm{pump}} \sin\varphi_{\mathrm{SHG}} \\
& + R_{ZYYXX} \cos\Omega_{\mathrm{SHG}} \sin^2\Omega_{\mathrm{VIS}} \cos^2\Omega_{\mathrm{pump}} \sin\varphi_{\mathrm{SHG}} \cos^2\varphi_{\mathrm{pump}} \\
& + R_{ZXXZZ} \cos\Omega_{\mathrm{SHG}} \cos^2\Omega_{\mathrm{VIS}} \cos^2\Omega_{\mathrm{pump}} \sin\varphi_{\mathrm{SHG}} \cos^2\varphi_{\mathrm{VIS}} \sin^2\varphi_{\mathrm{pump}} \\
& + R_{ZXXYY} \cos\Omega_{\mathrm{SHG}} \cos^2\Omega_{\mathrm{VIS}} \sin^2\Omega_{\mathrm{pump}} \sin\varphi_{\mathrm{SHG}} \cos^2\varphi_{\mathrm{VIS}} \\
& + R_{ZXXXX} \cos\Omega_{\mathrm{SHG}} \cos^2\Omega_{\mathrm{VIS}} \cos^2\Omega_{\mathrm{pump}} \sin\varphi_{\mathrm{SHG}} \cos^2\varphi_{\mathrm{VIS}} \cos^2\varphi_{\mathrm{pump}} \\
& + R_{YZYZZ} \sin\Omega_{\mathrm{SHG}} \cos\Omega_{\mathrm{VIS}} \sin\Omega_{\mathrm{VIS}} \cos^2\Omega_{\mathrm{pump}} \sin\varphi_{\mathrm{VIS}} \sin^2\varphi_{\mathrm{pump}} \\
& + R_{YZYYY} \sin\Omega_{\mathrm{SHG}} \cos\Omega_{\mathrm{VIS}} \sin\Omega_{\mathrm{VIS}} \sin^2\Omega_{\mathrm{pump}} \sin\varphi_{\mathrm{VIS}} \\
& + R_{YZYXX} \sin\Omega_{\mathrm{SHG}} \cos\Omega_{\mathrm{VIS}} \sin\Omega_{\mathrm{VIS}} \cos^2\Omega_{\mathrm{pump}} \sin\varphi_{\mathrm{VIS}} \cos^2\varphi_{\mathrm{pump}} \\
& + R_{XZXZZ} \cos\Omega_{\mathrm{SHG}} \cos^2\Omega_{\mathrm{VIS}} \cos^2\Omega_{\mathrm{pump}} \cos\varphi_{\mathrm{SHG}} \sin\varphi_{\mathrm{VIS}} \cos\varphi_{\mathrm{VIS}} \sin^2\varphi_{\mathrm{pump}} \\
& + R_{XZXYY} \cos\Omega_{\mathrm{SHG}} \cos^2\Omega_{\mathrm{VIS}} \sin^2\Omega_{\mathrm{pump}} \cos\varphi_{\mathrm{SHG}} \sin\varphi_{\mathrm{VIS}} \cos\varphi_{\mathrm{VIS}} \\
& + R_{XZXXX} \cos\Omega_{\mathrm{SHG}} \cos^2\Omega_{\mathrm{VIS}} \cos^2\Omega_{\mathrm{pump}} \cos\varphi_{\mathrm{SHG}} \sin\varphi_{\mathrm{VIS}} \cos\varphi_{\mathrm{VIS}} \cos^2\varphi_{\mathrm{pump}} \\
& + R_{YYZZZ} \sin\Omega_{\mathrm{SHG}} \sin\Omega_{\mathrm{VIS}} \cos\Omega_{\mathrm{VIS}} \cos^2\Omega_{\mathrm{pump}} \sin\varphi_{\mathrm{VIS}} \sin^2\varphi_{\mathrm{pump}} \\
& + R_{YYZYY} \sin\Omega_{\mathrm{SHG}} \sin\Omega_{\mathrm{VIS}} \cos\Omega_{\mathrm{VIS}} \sin^2\Omega_{\mathrm{pump}} \sin\varphi_{\mathrm{VIS}} \\
& + R_{YYZXX} \sin\Omega_{\mathrm{SHG}} \sin\Omega_{\mathrm{VIS}} \cos\Omega_{\mathrm{VIS}} \cos^2\Omega_{\mathrm{pump}} \sin\varphi_{\mathrm{VIS}} \cos^2\varphi_{\mathrm{pump}} \\
& + R_{XXZZZ} \cos\Omega_{\mathrm{SHG}} \cos\Omega_{\mathrm{VIS}} \cos\Omega_{\mathrm{VIS}} \cos^2\Omega_{\mathrm{pump}} \sin\varphi_{\mathrm{SHG}} \cos\varphi_{\mathrm{VIS}} \sin\varphi_{\mathrm{VIS}} \sin^2\varphi_{\mathrm{pump}} \\
& + R_{XXZYY} \cos\Omega_{\mathrm{SHG}} \cos\Omega_{\mathrm{VIS}} \cos\Omega_{\mathrm{VIS}} \sin^2\Omega_{\mathrm{pump}} \sin\varphi_{\mathrm{SHG}} \cos\varphi_{\mathrm{VIS}} \sin\varphi_{\mathrm{VIS}} \\
& + R_{XXZXX} \cos\Omega_{\mathrm{SHG}} \cos\Omega_{\mathrm{VIS}} \cos\Omega_{\mathrm{VIS}} \cos^2\Omega_{\mathrm{pump}} \sin\varphi_{\mathrm{SHG}} \cos\varphi_{\mathrm{VIS}} \sin\varphi_{\mathrm{VIS}} \cos^2\varphi_{\mathrm{pump}}
\end{aligned}
$$

calculated according to Table II. In Sec. IV, calculations are presented to demonstrate the dependence of the signal on the orientational diffusion constant and the cone half-angle.

IV. MODEL CALCULATIONS AND ANALYSIS OF EXPERIMENTS

A. Dependence of the observables on the cone half-angle

The effects of varying the diffusion constant and the cone half-angle will be demonstrated by calculating the orientational correlation function for a particular polarization combination, that is, the tensor elements for the circularly polarized pump scheme. Here, for simplicity, we will take the excited state life time to be long compared to the orientational relaxation, and leave it out of the calculations. Because the orientational motion is decoupled from the vibronic degrees of freedom [see Eq. (7)], the effect of the vibrational or electronic relaxation can be included by multiplying by the exponential population decay

$$\mathbf{R}^{\mathrm{L}}_{\eta\delta\gamma\alpha\alpha}(t) = \exp(-k_R t)\mathbf{R}_{\eta\delta\gamma\alpha\alpha}(t), \tag{56}$$

where k_R is the excited state relaxation rate and the superscript L indicates that the population decay is included. An excited state lifetime much longer than the orientational relaxation time scale commonly occurs in a TRSHG experiment.[25]

The simplest experimental scheme has the pump beam incident normal to the sample surface and circularly polarized in the plane of the surface.[19,25] The pump pulse electronically excites the molecules through an allowed one-photon absorption. The conical volume of the diffusion is assumed to be a cone whose symmetry axis is aligned along the surface normal. The lifetime decay is not included. When this approximation is invalid, it is necessary to measure decays at multiple pump-probe polarization conditions to separate the orientational decay from the population decay. For TRSHG and TRSFG experiments there is no analog to the anisotropy $r(t)$ [Eq. (1)].

To perform the model calculations, we use the equations that were derived for the orientational correlation functions and are listed in Table II. For the calculations, the input parameters are the cone half-angle, the orientational diffusion constant, and the molecular polarizability. All the calculations are for the case when the probe beam is two-photon resonant with an electronic excited state of the molecule. For example, the pump pulse is at 400 nm and the probe pulse is at 800. The electronic transition is both one-photon and two-photon resonant.

Figure 3 shows the simulated R_{ZYYCC} tensor component of the orientational correlation function. The diffusion constant is set to a value of 10^{-3} ps^{-1}, which is a realistic value

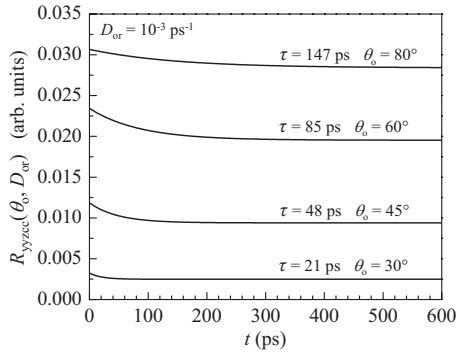

FIG. 3. The R^{SHG}_{YYZCC} tensor element is calculated for different cone semiangles and shown as a decay. The bleach in the visible-pump-SHG experiment is shown. The diffusion constant is set to an arbitrary but realistic value (D=10^{-3} ps^{-1}), while the cone semiangle is varied between 30° and 80°. The SHG/SFG signal always recovers exponentially to an equilibrium value. The exponential time constant of each decay is indicated in the figure; it is clear that the apparent time constant and the offset both depend strongly on the cone half-angle.

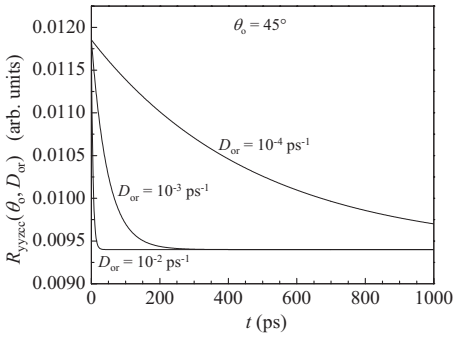

FIG. 4. The R^{SHG}_{YYZCC} tensor element calculated for different diffusion constants. The bleach in the visible-pump-SHG experiment is shown. The cone half-angle is set to θ_o=45°, while the diffusion constant is varied 10^{-4}–10^{-2} ps^{-1}. The SHG/SFG signal always recovers to the same equilibrium value independently of the diffusion constant. If it is assumed that $\tau = 1/6D_{or}$, the obtained diffusion constant is larger by a factor of 3.5 from what was used in the simulations.

for molecules like Rhodamine 6G (Ref. 19) or C314 (Ref. 27), for example. The isotropic part of the polarizability is set to 1, and the anisotropic part is set to 1/3, that is, the anisotropic-isotropic ratio is one third. The cone semiangle is varied between 30° and 80°. Before t=0, the SHG signal of the sample is recorded. When the pump beam is turned on, the SHG signal decreases, and it recovers to the equilibrium value over time. As an example, the R^{SHG}_{YYZCC} response function is plotted as a function of the pump-probe delay time in Fig. 3. Each of the signal decay curves is a single exponential that decays to an offset. Both the decay constant and the offset depend both on the orientational diffusion constant and the cone half-angle. In Fig. 3, all of the curves are calculated for the same diffusion constant, $D_{or}=10^{-3}$ ps^{-1}. The cone half-angles are varied as shown in the figure. To obtain a feel for how much the cone half-angle influences the experimentally observed decay time, the curves were fit to exponential decays to an offset. The results are dramatic. Although D_{or} is the same for all curves, the apparent decay time constants range from 21 (θ_o=30°) to 147 ps (θ_o=80°). It is clear from these model calculations that the decay constant alone cannot provide microscopic information on the orientational dynamics. However, as discussed in Sec. IV B, if the cone half-angle is known from time-independent measurements,[11] then measurement of the decay does permit the determination of the orientational diffusion constant.

The theory shows that it is not necessary to make a separate static measurement of the cone half-angle. It is possible to obtain both the orientational diffusion constant and the cone half-angle from the time-dependent experiment alone. In Fig. 3, the initial amplitude of the signal varies with the cone half-angle. In addition, the ratio of the initial value (t=0) and the long time plateau amplitude is sufficient to determine the cone half-angle. With the cone half-angle and the decay constant, the orientational diffusion constant can be determined.

Figure 4 shows three decay curves for the same cone half-angle 45°, but with diffusion constants varying by two orders of magnitude 10^{-2}–10^{-4} ps^{-1}. The figure shows several important points. First, for the same cone half-angle, the initial value of the signal is the same independent of the diffusion constant. Furthermore, the plateau level is the same for all three curves, although the slowest decay in the figure has not reached this plateau in the time range displayed. As discussed in connection with Fig. 3, the initial value and the plateau value are sufficient to determine the cone half-angle. With the cone half-angle and the decay time constant, the orientational diffusion constant D_{or} can be determined.

If the decays in Fig. 4 are fit to an exponential decaying to a constant, and the decay time constant is taken to be $\tau = 1/6D$, as it would be in a bulk liquid, the diffusion constants are always a factor of 3.5 larger than the diffusion constant used to calculate the decays. For other cone half-angles, the factor is different as is clear from Fig. 3. As with Fig. 3, Fig. 4 shows that it is not possible to determine the orientational diffusion constant from a measurement of the decay time. Furthermore, Figs. 3 and 4 demonstrate that decay times measured on different systems, which can have different cone half-angles, cannot be directly compared.

B. A realistic example: TRSHG measurements on the C314 monolayer

Above, calculations were presented with several diffusion constants and half-cone angles to illustrate how the observables depend on both of these physical parameters. Here we examine a system that has been examined experimentally. Eisenthal and co-workers studied C314 at the air/water interface of an aqueous solution by TRSHG[24,25] and TRSFG (Ref. 22) experiments as well as in bulk water.[59] In bulk water, the orientational relaxation time constant was found to be 106 ps.[60] The surface relaxation time constant was also measured at the air/water interface, and it was found to be 350 ps.[24] From the comparison of the measured time constants, the authors concluded that the orientational diffusion is significantly slower at the interface.

Nguyen *et al.*[25] modified the surface by adding the surfactant sodium dodecyl sulfate (SDS) to the C314 solution. SDS forms a monolayer at the air-water interface. At the surface, the C314 orientational time constant was found to be very similar to the interface without the surfactant, only increasing 15% to 383 ps. From the time constants, it was concluded that modifying the surface changes the C314 orientational diffusion only slightly.

By using Eq. (3), the diffusion constant in the bulk phase can be obtained, and it is 1.6×10^{-3} ps^{-1}. To obtain the diffusion constants at the interfaces, we use the equations derived above. In the analysis, we employ the previously published experimental data[24,25] to demonstrate how the orientational correlation functions along with the wobbling-in-a-cone model can be used to obtain the orientational diffusion constants at the air-water interface and the air-water-surfactant interface. Eisenthal and co-workers[25] measured the SHG signal using the $\chi^{(2)}_{XZX}$ and $\chi^{(2)}_{ZXX}$ susceptibility tensor elements, and found identical reorientational dynamics for both tensor elements. They report that after excitation, the SHG signal decreases and it recovers exponentially to an equilibrium value. The time-dependent signal can be fit with a single exponential decay plus a constant. At the air-water

interface, the time constant of the single exponential decay is 350 ps, and the remaining bleach is approximately 20%. The exact number of the offset was not reported.

To use the equations derived above, one needs the cone half-angle through which restricted diffusion occurs. In principle, the cone half-angle can be obtained from the offset of the exponential decay (see Figs. 3 and 4). In this case, only an approximate value of the offset was reported. The cone half-angle can also be obtained from the average orientational angle which was determined in static experiments.[25] In Eqs. (15) and (16), we show that the average orientational angle of the molecules at the surface can be related to the cone half-angle by an orientational average. At the air-water interface, the measured average polar angle of the C314 molecules is 67°,[25] which corresponds to a cone half-angle of 102°, a reasonable value. In molecular dynamics studies, it was found that at the air-water interface the C314 molecules can lie in the plane of the surface and also that the less polar end of the molecule can rotate to penetrate into the bulk phase.[61,62]

From the equations in Table II, one can see that the combination of the $\langle Y_1^0 Y_2^0 \rangle$ and $\langle Y_3^0 Y_2^0 \rangle$ correlation functions are measured by the experiment. We assume that the symmetry axis of the cone of the diffusion is the surface normal and the dipole moment of C314 lies in the molecular plane. Therefore, the correlation functions decay as single exponentials in every combination as observed. The decay rate is $\nu_2^0(\nu_2^0+1)D_{\mathrm{or}}$. The coefficients in the time constant can be calculated from the cone half-angle by Eq. (54). For the cone half-angle of 102° determined from the static measurements and time constant of 350 ps determined from the dynamical measurements, the diffusion constant is $D_{\mathrm{or}}=6.6\times10^{-4}$ ps^{-1}. This diffusion constant for the air-water interface should be compared to the one measured in bulk water of 1.6×10^{-3} ps^{-1}. This result shows that the reorientation of the C314 molecules slows down at the air-water interface by a factor of 2.5.

Now, we examine the surface modified with SDS. SDS forms a monolayer at the air-water interface. The rotational time constant was found to increase only by 15% to 383 ps at the air-water-surfactant interface compared to the time constant measured for the pure air-water interface. However, the static measurements showed that the equilibrium orientational angle of the C314 molecules with the surfactant changed substantially to 45° compared the 67° in the absence of the surfactant.[25] As shown in Fig. 3, the cone angle plays an important role in the observed orientational decay time. Using the method outlined above, the orientational diffusion constant of C314 is found to be 2.6×10^{-4} ps^{-1} at the air-water-surfactant interface compared to 6.6×10^{-4} ps^{-1} at the air-water interface. This is almost a *threefold decrease* that is not reflected in the measured time constants. Here, we followed the literature and have assumed that the tilt angle does not change upon surface modification, that is, the axis of the cone is still normal to the surface. These results are also physically intuitive. In the case of the SDS modified surface, the molecular orientational response decays with an experimental rate similar to that for the unmodified interface; however, the chromophore traverses a smaller solid angle. This suggests intuitively that the measured diffusion constant should be smaller, which is exactly what the formal theoretical treatment proves.

The net result of the analysis that yields the orientational diffusion constants is to come to conclusions that are very different from those obtained by only comparing the time constants. We have determined that the addition of the surfactant substantially reduces the interfacial diffusion constant.

V. CONCLUDING REMARKS

TRSHG and TRSFG experiments have proven to be useful tools in investigating the orientational dynamics of molecules at interface. However, little was known about the specific correlation functions measured in the experiments. Some authors interpreted data without accounting for the effects of the restricted rotational diffusion. Others used numerical simulation methods that do not permit a general analysis of the experiments.

In the work presented here, we calculated the orientational correlation functions for the TRSHG and TRSFG experiments. The derivations were performed in general, and then specific results were obtained for interfacial molecules that can be approximated as rigid rods with cylindrical symmetry. The derivations are valid for resonant experiments, when the probe beam is either in one-photon or two-photon resonance with the electronic or vibrational transition of the molecules under investigation.

The theoretical results show that TRSHG and TRSFG experiments measure a linear combination of the $\langle Y_l^m(\Omega_{\mathrm{lab}}(t))Y_2^m(\Omega_{\mathrm{lab}}(0))\rangle$ ($l=1,3$ and $m=0,1,2$) orientational correlation functions. To evaluate the correlation functions, we applied the wobbling-in-a-cone model, which describes the reorientational motion of the molecules diffusing in a restricted range of angles, the cone. This model was successfully applied to a number of systems in the bulk phase.[31,42,52–55] For the case when the $C_{\infty v}$ symmetry axis of the cone is not the surface normal, the correlation function written in the laboratory coordinates was transformed into the coordinate system fixed to the conical volume of the diffusion. This transformation permits the general treatment of any spectroscopic probe at an interface regardless of its mean orientation angle.

The analytical treatment presented here can be extended to incorporate any model of diffusion including diffusion models with explicit potential functions. As long as a Green's function can be solved for analytically or numerically, the correlation functions that have been derived can be calculated and compared to experimental data. Given an experimental configuration, it is now possible to choose the proper correlation functions to calculate and to calculate them with an appropriate Green's function.

The general correlation functions derived in this work are also useful for those simulating interfacial molecular systems. Now there exists a clear link between the TRSHG and TRSFG experiments and correlation functions which can be readily calculated with molecular dynamics simulations. Even when diffusion and other dynamic models fail, molecu-

lar dynamics simulations can be linked directly to experimental data through the correlation functions. This linkage enables the validity of simulation models to be tested.

The application of the wobbling-in-a-cone model lead to analytical expressions of the orientational correlation functions, and it was found that they can always be expressed as a single exponential decay to an offset, which is in agreement with the experimental findings.[25] The analytical expressions were used to analyze the results of experiments from the literature for a chromophore at the air-water interface and at the air-water-surfactant interface.[25] By using both the experimentally determined decay time and cone half-angle, the interfacial orientational diffusion constants were obtained. The diffusion constants showed that the diffusion constant of C314 at the air-water is smaller than its bulk value. Adding an interfacial layer of the surfactant SDS reduced the diffusion constant by about a factor of 3, which is in contrast to the conclusions obtained by comparing the experimentally observed decay time constants. As illustrated in Figs. 3 and 4, the determining the orientational diffusion constant requires both the decay time and the cone half-angle in addition to the use of the detailed theory.

It is important to emphasize that a direct comparison of the orientational time constants of TRSHG or TRSFG experiments to bulk orientational decay constants, or orientational decay constants from interfaces with different mean orientation angles, will *not* result in a valid comparison of orientational dynamics. We examined uniform angular distribution functions in confined solid angles for mathematical simplicity. Other models can be used within the same theoretical framework. The theoretical results also demonstrate the utility of using dynamics as a probe of the angular distribution of chromophores. A significant problem in interfacial spectroscopy is the independent determination of both mean angle and angular distribution. Dynamical measurements and their proper interpretation via diffusion models can enable information to be gathered not only about the motion of molecules at interfaces but also their average structure. Such measurements can provide detailed insights into the chemistry and physics of interfacial systems.

Note added in proof. As discussed in the text, for TRSFG the results are obtained when the transition polarizability tensor (the derivative of the polarizability tensor taken at the equilibrium geometry) is diagonal. The results apply if the vibrational mode is totally symmetric and the transition dipole moment is along the principle axis of the polarizability ellipsoid. The results can be readily generalized to vibrations with symmetries other than totally symmetric by choosing a transition polarizability tensor with the appropriate symmetry. For totally symmetric vibrations, the symmetry of the polarizability tensor and its derivative are the same.

ACKNOWLEDGMENTS

This research was supported by a grant from the Air Force Office of Scientific Research (Grant No. F49620-01-1-0018). D.E.R. thanks the Fannie and John Hertz Foundation, the Stanford Graduate Fellowship program, and the National Science Foundation Graduate Research Fellowship Program for fellowships.

APPENDIX A: THE CORRELATION FUNCTIONS IN THE WOBBLING-IN-A-CONE MODEL

In this Appendix, we derive the $\langle Y_l^{m^*}(\Omega(t))Y_2^m(\Omega(0))\rangle$ $\langle Y_l^{m^*}(\Omega(t))Y_2^m(\Omega(0))\rangle$ correlation functions and show that they are well represented by keeping terms only to the first decaying exponential. Using the equations

$$\begin{aligned}\langle Y_l^{m^*}(\Omega(t))Y_{l'}^{m'}(\Omega(0))\rangle &= \langle Y_l^{-m^*}(\Omega(t))Y_{l'}^{-m'}(\Omega(0))\rangle \\ &= \frac{\delta_{mm'}}{4\pi}\sqrt{\frac{(2l+1)(2l'+1)(l-m)!(l'-m)!}{(l+m)!(l'+m)!}} \\ &\quad\times\sum_{n=1}^{\infty} C_n^m \exp(-\nu_n^m(\nu_n^m+1)D_{\mathrm{or}}t)\end{aligned} \tag{A1}$$

and

$$\begin{aligned}C_n^m = \frac{1}{H_n^m(1-\cos\theta_{\mathrm{o}})}\int_0^{\theta_{\mathrm{o}}} d\theta \sin\theta P_l^m(\cos\theta)P_{\nu_n^m}^m(\cos\theta) \\ \times\int_0^{\theta_{\mathrm{o}}} d\theta' \sin\theta' P_{l'}^m(\cos\theta')P_{\nu_n^m}^m(\cos\theta'),\end{aligned} \tag{A2}$$

the C_n^m coefficients can be easily calculated. H_n^m denotes the overlap integrals of the associated Legendre polynomials

$$H_n^m = \int_0^{\theta_{\mathrm{o}}} d\theta \sin\theta P_{\nu_n^m}^m(\cos\theta)P_{\nu_n^m}^m(\cos\theta'). \tag{A3}$$

We can use that for all θ_{o}

$$\nu_1^0 = 0 \tag{A4}$$

and

$$P_{\nu_1^0}^0(\cos\theta_{\mathrm{o}}) = 1. \tag{A5}$$

This leads to

$$H_1^0 = 1-\cos\theta_{\mathrm{o}}. \tag{A6}$$

At $t=0$, the correlation function is given as

$$\begin{aligned}\langle Y_l^{m^*}(\Omega(0))Y_{l'}^{m'}(\Omega(0))\rangle = \frac{1}{2\pi(1-\cos\theta_{\mathrm{o}})}\int_0^{2\pi} d\phi\int_0^{\theta_{\mathrm{o}}} d\theta \\ \times\sin\theta Y_l^{m^*}(\Omega(0))Y_{l'}^{m'^*}(\Omega(0)),\end{aligned} \tag{A7}$$

which is equal to the infinite sum of the exponential coefficients

$$\langle Y_l^{m^*}(\Omega(0))Y_{l'}^m(\Omega(0))\rangle = \sum_{n=1}^{\infty} C_n^m. \tag{A8}$$

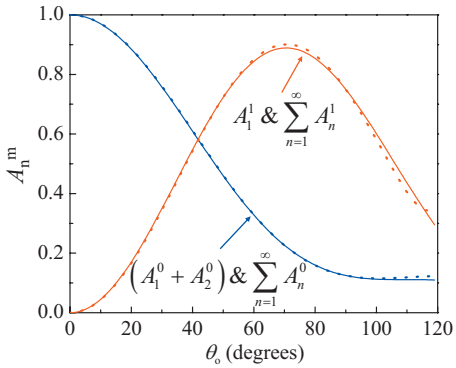

FIG. 5. The A_n^m parameters of the $\langle Y_1^{m^*}(\Omega(t))Y_2^m(\Omega(0))\rangle$ correlation functions. The solid lines are calculated from Eqs. (A11) and (A12) for the sum rules. The dashed lines are calculated for $A_1^0+A_2^0$ and A_1^1 numerically. See details in text.

1. The $\langle Y_1^{m^*}(\Omega(t))Y_2^m(\Omega(0))\rangle$ correlation functions

From Eqs. (A1) and (A2), the dynamic ensemble averages can be written as

$$\langle Y_1^{0^*}(\Omega(t))Y_2^0(\Omega(0))\rangle = \frac{\sqrt{15}}{4\pi}\sum_{n=1}^{\infty} A_n^0 \exp[-\nu_n^0(\nu_n^0+1)D_{or}t] \tag{A9}$$

and

$$\langle Y_1^{1^*}(\Omega(t))Y_2^1(\Omega(0))\rangle = \frac{\sqrt{5}}{8\pi}\sum_{n=1}^{\infty} A_n^1 \exp[-\nu_n^1(\nu_n^1+1)D_{or}t]. \tag{A10}$$

The sum rules can be obtained by setting $t=0$.

$$\langle Y_1^{0^*}(\Omega(0))Y_2^0(\Omega(0))\rangle = \frac{\sqrt{15}}{4\pi}\sum_{n=1}^{\infty} A_n^0 = \frac{\sqrt{15}}{4\pi}\frac{(5+3\cos(2\theta_o))\sin^2\theta_o}{16(1-\cos\theta_o)} \tag{A11}$$

and

$$\langle Y_1^{1^*}(\Omega(0))Y_2^1(\Omega(0))\rangle = \frac{\sqrt{5}}{8\pi}\sum_{n=1}^{\infty} A_n^1 = \frac{\sqrt{5}}{8\pi}\frac{3\sin^4\theta_o}{4(1-\cos\theta_o)}. \tag{A12}$$

From Eqs. (A4)–(A6), A_1^0 can be calculated analytically

$$A_1^0 = \tfrac{1}{4}\cos\theta_o(1+\cos\theta_o)^2, \tag{A13}$$

while the $A_n^m(m\neq 0 \text{ or } n\geq 2)$ coefficients can be calculated only numerically. In Fig. 5, plots of $\Sigma_{n=1}^{\infty}A_n^0$, A_1^0, A_2^0, $\Sigma_{n=1}^{\infty}A_n^1$, and A_1^1 are shown.

Figure 5 shows that for $\theta_o \leq 120°$,

$$A_2^0 \approx \sum_{n=2}^{\infty} A_n^0 = \sum_{n=1}^{\infty} A_n^0 - A_1^0 = \frac{1}{4}\sin^2\frac{\theta_o}{2}\sin^2\theta_o \tag{A14}$$

and

$$A_1^1 \approx \sum_{n=1}^{\infty} A_n^1 = \frac{3\sin^4\theta_o}{4(1-\cos\theta_o)}. \tag{A15}$$

Because $\nu_1^0=0$ and $\exp[-\nu_1^0(\nu_1^0+1)D_{or}t]=1$, only the first two terms in Eq. (A9) contribute meaningfully, and the correlation functions can be written as

$$\langle Y_1^{0^*}(\Omega(t))Y_2^0(\Omega(0))\rangle = \frac{\sqrt{15}}{4\pi}(A_1^0+A_2^0)\exp[-\nu_2^0(\nu_2^0+1)D_{or}t] \tag{A16}$$

and

$$\langle Y_1^{1^*}(\Omega(t))Y_2^1(\Omega(0))\rangle = \frac{\sqrt{5}}{8\pi}A_1^1 \exp[-\nu_1^1(\nu_1^1+1)D_{or}t]. \tag{A17}$$

2. The $\langle Y_3^{m^*}(\Omega(t))Y_2^m(\Omega(0))\rangle$ correlation functions

Let us write the dynamic ensemble averages as

$$\langle Y_3^{0^*}(\Omega(t))Y_2^0(\Omega(0))\rangle = \frac{\sqrt{35}}{4\pi}\sum_{n=1}^{\infty} B_n^0 \exp[-\nu_n^0(\nu_n^0+1)D_{or}t], \tag{A18}$$

$$\langle Y_3^{1^*}(\Omega(t))Y_2^1(\Omega(0))\rangle = \frac{\sqrt{35}}{24\sqrt{2}\pi}\sum_{n=1}^{\infty} B_n^1 \exp[-\nu_n^1(\nu_n^1+1)D_{or}t], \tag{A19}$$

and

$$\langle Y_3^{2^*}(\Omega(t))Y_2^2(\Omega(0))\rangle = \frac{\sqrt{7}}{96\pi}\sum_{n=1}^{\infty} B_n^2 \exp[-\nu_n^2(\nu_n^2+1)D_{or}t]. \tag{A20}$$

Following the above applied procedure, first we find the sum rules are

$$\langle Y_3^{0^*}(\Omega(0))Y_2^0(\Omega(0))\rangle = \frac{\sqrt{35}}{4\pi}\sum_{n=1}^{\infty} B_n^0 = \frac{1}{32}\cos^2\frac{\theta_o}{2}(12\cos 2\theta_o + 5(3+\cos 4\theta_o)), \tag{A21}$$

$$\langle Y_3^{1^*}(\Omega(0))Y_2^1(\Omega(0))\rangle = \frac{\sqrt{35}}{24\sqrt{2}\pi}\sum_{n=1}^{\infty} B_n^1 = \frac{3}{8}\frac{(7+5\cos 2\theta_o)\sin^4\theta_o}{1-\cos\theta_o}, \tag{A22}$$

and

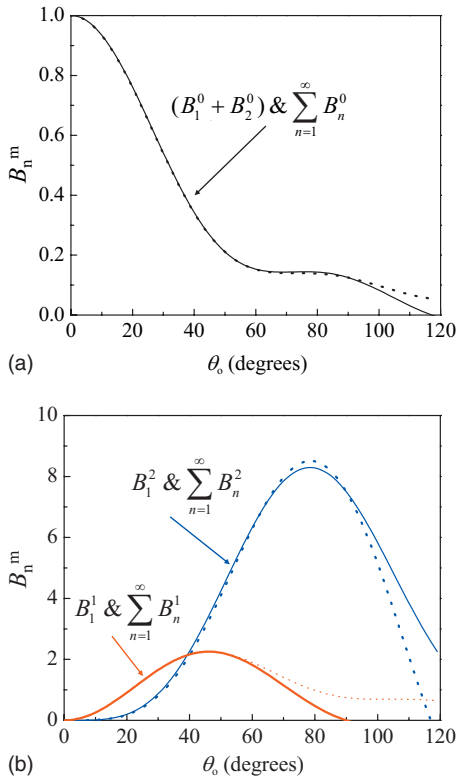

FIG. 6. [(a) and (b)] The B_n^m parameters of the $\langle Y_3^{m^*}(\Omega(t))Y_2^m(\Omega(0))\rangle$ correlation functions. The solid lines are calculated from Eqs. (A21) and (A22) for the sum rules. The dashed lines are calculated for $B_1^0+B_2^0$, B_1^1, and B_1^2 numerically. See details in text.

$$\langle Y_3^{2^*}(\Omega(0))Y_2^2(\Omega(0))\rangle = \frac{\sqrt{7}}{96\pi}\sum_{n=1}^{\infty} B_n^2 = \frac{15}{2}\frac{\sin^6\theta_o}{1-\cos\theta_o}. \tag{A23}$$

Again, from Eqs. (A4)–(A6) B_1^0 can be calculated analytically

$$B_1^0 = \frac{1}{16}\cos\theta_o(1+\cos\theta_o)^2(5\cos^2\theta_o - 1), \tag{A24}$$

while the $B_n^m (m \neq 0 \text{ or } n \geq 2)$ coefficients can be calculated only numerically. In Fig. 6, plots of $\Sigma_{n=1}^{\infty}B_n^0$, B_1^0, B_2^0; $\Sigma_{n=1}^{\infty}B_n^1$, B_1^1, B_2^1; and $\Sigma_{n=1}^{\infty}B_n^2$, B_1^2 are shown. Figure 6 shows that for $\theta_o < 110°$,

$$B_2^0 \approx \sum_{n=2}^{\infty} B_n^0 = \sum_{n=1}^{\infty} B_n^0 - B_1^0 = \frac{1}{4}\cos^2\frac{\theta_o}{2}(9+10\cos\theta_o+5\cos 2\theta_o)\sin^4\frac{\theta_o}{2} \tag{A25}$$

and

$$B_1^2 \approx \sum_{n=1}^{\infty} B_n^1 = \frac{15}{2}\frac{\sin^6\theta_o}{1-\cos\theta_o}. \tag{A26}$$

Using that $\nu_1^0=0$ and $\exp[-\nu_1^0(\nu_1^0+1)D_{or}t]=1$ and approximations above, the correlation functions can be written as

$$\langle Y_3^{0^*}(\Omega(t))Y_2^0(\Omega(0))\rangle = \frac{\sqrt{35}}{4\pi}(B_1^0+B_2^0)\exp[-\nu_2^0(\nu_2^0+1)D_{or}t], \tag{A27}$$

$$\langle Y_3^{1^*}(\Omega(t))Y_2^1(\Omega(0))\rangle = \frac{\sqrt{35}}{24\sqrt{2}\pi}B_1^1\exp[-\nu_1^1(\nu_1^1+1)D_{or}t], \quad (\text{for } \theta_o < 70° \text{ only}), \tag{A28}$$

and

$$\langle Y_3^{2^*}(\Omega(t))Y_2^2(\Omega(0))\rangle = \frac{\sqrt{7}}{96\pi}B_1^2\exp[-\nu_1^2(\nu_1^2+1)D_{or}t]. \quad (\text{for } \theta_o < 110° \text{ only}). \tag{A29}$$

APPENDIX B: ALGEBRAIC TRANSFORMATIONS OF THE SPHERICAL HARMONIC FUNCTIONS

The evaluation of the orientational correlation functions requires algebraic transformation of the spherical harmonic representations of the field-matter interactions. Using simple relationships between spherical harmonics of different order, those representations can always be written as the sum of a constant and spherical harmonics of the order of one to three. The pump field can be polarized along any of the Cartesian coordinate axis, and we also consider the case when it propagates along the Z axis and is circularly polarized in the XY plane. Because the pump interaction is approximated as instantaneous, the pump field-matter interaction can be written for different polarizations as

$$(\mu_i\hat{\varepsilon}_Z)^2 = \frac{1}{3}+\frac{4}{3}\sqrt{\frac{\pi}{5}}Y_2^0(\Omega(t_i)), \tag{B1}$$

$$(\hat{\mu}_i\hat{\varepsilon}_Y)^2 = \frac{1}{3}-\frac{2}{3}\sqrt{\frac{\pi}{5}}Y_2^0(\Omega(t_i)) - \sqrt{\frac{2\pi}{15}}(Y_{-2}^2(\Omega(t_i)) + Y_2^2(\Omega(t_i))), \tag{B2}$$

$$(\hat{\mu}_i\hat{\varepsilon}_X)^2 = \frac{1}{3}-\frac{2}{3}\sqrt{\frac{\pi}{5}}Y_2^0(\Omega(t_i)) + \sqrt{\frac{2\pi}{15}}(Y_{-2}^2(\Omega(t_i)) + Y_2^2(\Omega(t_i))), \tag{B3}$$

and

$$(\hat{\mu}_i\hat{\varepsilon}_{\text{CIRC}})^2 = \frac{2}{3}-\frac{4}{3}\sqrt{\frac{\pi}{5}}Y_2^0(\Omega(t_i)). \tag{B4}$$

In the probe interactions, only the polarization combinations that are allowed by the symmetry of the surface are considered.

$$(\hat{\mu}_i\hat{\varepsilon}_Z\hat{\varepsilon}_Z\hat{\alpha}_i\hat{\varepsilon}_Z) = (\hat{\varepsilon}_Z\hat{\alpha}_i\hat{\varepsilon}_Z\hat{\mu}_i\hat{\varepsilon}_Z) = \frac{2}{15}\sqrt{\frac{\pi}{3}}(15\alpha+4\beta)Y_1^0(\Omega(t_i)) + \frac{4}{5}\sqrt{\frac{\pi}{7}}\beta Y_1^0(\Omega(t_i)), \tag{B5}$$

$$(\hat{\mu}_i\hat{\varepsilon}_Z\hat{\varepsilon}_Y\hat{\alpha}_i\hat{\varepsilon}_Y) = (\hat{\varepsilon}_Y\hat{\alpha}_i\hat{\varepsilon}_Y\hat{\mu}_i\hat{\varepsilon}_Z)$$
$$= \frac{2}{15}\sqrt{\frac{\pi}{3}}(15\alpha - 2\beta)Y_1^0(\Omega(t_i))$$
$$- \beta\sqrt{\frac{2\pi}{105}}\beta(Y_3^{-2}(\Omega(t_i)) + Y_3^2(\Omega(t_i)))$$
$$- \frac{2}{5}\sqrt{\frac{\pi}{7}}\beta Y_3^0(\Omega(t_i)), \quad \text{(B6)}$$

$$(\hat{\mu}_i\hat{\varepsilon}_Z\hat{\varepsilon}_X\hat{\alpha}_i\hat{\varepsilon}_X) = (\hat{\varepsilon}_X\hat{\alpha}_i\hat{\varepsilon}_X\hat{\mu}_i\hat{\varepsilon}_Z)$$
$$= \frac{2}{15}\sqrt{\frac{\pi}{3}}(15\alpha - 2\beta)Y_1^0(\Omega(t_i))$$
$$+ \sqrt{\frac{2\pi}{105}}\beta(Y_3^{-2}(\Omega(t_i)) + Y_3^2(\Omega(t_i)))$$
$$- \frac{2}{5}\sqrt{\frac{\pi}{7}}\beta Y_3^0(\Omega(t_i)) \quad \text{(B7)}$$

$$(\hat{\mu}_i\hat{\varepsilon}_Y\hat{\varepsilon}_Y\hat{\alpha}_i\hat{\varepsilon}_Z) = (\hat{\mu}_i\hat{\varepsilon}_Y\hat{\varepsilon}_Z\hat{\alpha}_i\hat{\varepsilon}_Y)$$
$$= (\hat{\varepsilon}_Y\hat{\alpha}_i\hat{\varepsilon}_Z\hat{\mu}_i\hat{\varepsilon}_Y)$$
$$= (\hat{\varepsilon}_Z\hat{\alpha}_i\hat{\varepsilon}_Y\hat{\mu}_i\hat{\varepsilon}_Y)$$
$$= \frac{2}{5}\sqrt{\frac{\pi}{3}}\beta Y_1^0(\Omega(t_i)) - \sqrt{\frac{2\pi}{105}}\beta(Y_3^{-2}(\Omega(t_i))$$
$$+ Y_3^2(\Omega(t_i))) - \frac{2}{5}\sqrt{\frac{\pi}{7}}\beta Y_3^0(\Omega(t_i)) \quad \text{(B8)}$$

$$(\hat{\mu}_i\hat{\varepsilon}_X\hat{\varepsilon}_X\hat{\alpha}_i\hat{\varepsilon}_Z) = (\hat{\mu}_i\hat{\varepsilon}_X\hat{\varepsilon}_Z\hat{\alpha}_i\hat{\varepsilon}_X)$$
$$= (\hat{\varepsilon}_X\hat{\alpha}_i\hat{\varepsilon}_Z\hat{\mu}_i\hat{\varepsilon}_X)$$
$$= (\hat{\varepsilon}_Z\hat{\alpha}_i\hat{\varepsilon}_X\hat{\mu}_i\hat{\varepsilon}_X)$$
$$= \frac{2}{5}\sqrt{\frac{\pi}{3}}\beta Y_1^0(\Omega(t_i)) + \sqrt{\frac{2\pi}{105}}\beta(Y_3^{-2}(\Omega(t_i))$$
$$+ Y_3^2(\Omega(t_i))) - \frac{2}{5}\sqrt{\frac{\pi}{7}}\beta Y_3^0(\Omega(t_i)). \quad \text{(B9)}$$

[1] G. A. Somorjai, *Introduction to Surface Chemistry and Catalysis* (Wiley, New York, 1994).
[2] G. A. Somorjai, Annu. Rev. Phys. Chem. **45**, 721 (1994).
[3] T. Kakuchi, in *Interfacial Catalysis*, edited by A. G. Volkov (Dekker, New York, 2003).
[4] P. Moriarty, Rep. Prog. Phys. **64**, 297 (2001).
[5] R. G. Quiller, L. Benz, J. Haubrich, M. E. Colling, and C. M. Friend, J. Phys. Chem. C **113**, 2063 (2009).
[6] C. R. Usher, A. E. Michel, and V. H. Grassian, Chem. Rev. (Washington, D.C.) **103**, 4883 (2003).
[7] S. McLaughlin, Annu. Rev. Biophys. Biophys. Chem. **18**, 113 (1989).
[8] A. G. Volkov, D. W. Deamer, D. L. Tanelian, and V. S. Markin, *Liquid Interfaces in Chemistry and Biology* (Wiley, New York, 1998).
[9] Y. R. Shen, *The Principles of Nonlinear Optics* (Wiley, New York, 1984).
[10] R. W. Boyd, *Nonlinear Optics*, 3rd ed. (Elsevier, New York, 2008).
[11] H.-F. Wang, W. Gan, R. Lu, Y. Rao, and B.-H. Wu, Int. Rev. Phys. Chem. **24**, 191 (2005).
[12] X. Zhuang, P. B. Miranda, D. Kim, and Y. R. Shen, Phys. Rev. B **59**, 12632 (1999).
[13] Y. Rao, M. Comstock, and K. B. Eisenthal, J. Phys. Chem. B **110**, 1727 (2006).
[14] G. A. Somorjai and J. Y. Park, Surf. Sci. **603**, 1293 (2009).
[15] Y. R. Shen and V. Ostroverkhov, Chem. Rev. (Washington, D.C.) **106**, 1140 (2006).
[16] G. A. Somorjai and J. Y. Park, Chem. Soc. Rev. **37**, 2155 (2008).
[17] K. M. Bratlie, K. Komvopoulos, and G. A. Somorjai, J. Phys. Chem. C **112**, 11865 (2008).
[18] X. Wei and Y. R. Shen, Phys. Rev. Lett. **86**, 4799 (2001).
[19] A. Castro, E. V. Sitzmann, D. Zhang, and K. B. Eisenthal, J. Phys. Chem. **95**, 6752 (1991).
[20] R. Antoine, A. A. Tamburello-Luca, P. Hébert, P. F. Brevet, and H. H. Girault, Chem. Phys. Lett. **288**, 138 (1998).
[21] K. Sekiguchi, S. Yamaguchi, and T. Tahara, J. Chem. Phys. **128**, 114715 (2008).
[22] Y. Rao, D. Song, N. J. Turro, and K. B. Eisenthal, J. Phys. Chem. B **112**, 13572 (2008).
[23] J. A. McGuire and Y. R. Shen, Science **313**, 1945 (2006).
[24] D. Zimdars, J. I. Dadap, K. B. Eisenthal, and T. F. Heinz, J. Phys. Chem. B **103**, 3425 (1999).
[25] K. T. Nguyen, X. Shang, and K. B. Eisenthal, J. Phys. Chem. B **110**, 19788 (2006).
[26] M. J. Wirth and J. D. Burbage, J. Phys. Chem. **96**, 9022 (1992).
[27] X. Shang, K. Nguyen, Y. Rao, and K. B. Eisenthal, J. Phys. Chem. C **112**, 20375 (2008).
[28] H.-K. Nienhuys and M. Bonn, J. Phys. Chem. B **113**, 7564 (2009).
[29] M. P. Warchol and W. E. Vaughan, Adv. Mol. Relax. Interact. Processes **13**, 317 (1978).
[30] C. C. Wang and R. Pecora, J. Chem. Phys. **72**, 5333 (1980).
[31] A. Tokmakoff and M. D. Fayer, J. Chem. Phys. **103**, 2810 (1995).
[32] B. J. Berne and R. Pecora, *Dynamic Light Scattering: With Applications to Chemistry, Biology, and Physics* (Dover, Mineola, 2000).
[33] A. Szabo, J. Chem. Phys. **81**, 150 (1984).
[34] A. Tokmakoff, J. Chem. Phys. **105**, 1 (1996).
[35] T. Tao, Biopolymers **8**, 609 (1969).
[36] P. J. W. Debye, *Polar Molecules* (Dover, New York, 1945).
[37] A. Carrington and A. D. McLachlan, *Introduction to Magnetic Resonance with Applications to Chemistry and Chemical Physics* (Harper & Row, New York, 1967).
[38] A. Tokmakoff, R. S. Urdahl, D. Zimdars, R. S. Francis, A. S. Kwok, and M. D. Fayer, J. Chem. Phys. **102**, 3919 (1995).
[39] J. M. Beechem and L. Brand, Annu. Rev. Biochem. **54**, 43 (1985).
[40] R. E. Dale, S. C. Hopkins, U. A. an der Heide, T. Marszalek, M. Irving, and Y. E. Goldman, Biophys. J. **76**, 1606 (1999).
[41] H. Vogel and F. Jahnig, Proc. Natl. Acad. Sci. U.S.A. **82**, 2029 (1985).
[42] I. R. Piletic, D. E. Moilanen, D. B. Spry, N. E. Levinger, and M. D. Fayer, J. Phys. Chem. A **110**, 4985 (2006).
[43] A. Szabo, J. Chem. Phys. **72**, 4620 (1980).
[44] D. E. Moilanen, E. E. Fenn, Y. S. Lin, J. L. Skinner, B. Bagchi, and M. D. Fayer, Proc. Natl. Acad. Sci. U.S.A. **105**, 5295 (2008).
[45] S. Mukamel, *Principles of Nonlinear Optical Spectroscopy* (Oxford University Press, New York, 1995).
[46] S. Mukamel and R. F. Loring, J. Opt. Soc. Am. B **3**, 595 (1986).
[47] A. Tokmakoff, J. Chem. Phys. **105**, 13 (1996).
[48] S. Park, K. Kwak, and M. D. Fayer, Laser Phys. Lett. **4**, 704 (2007).
[49] M. Cho, G. R. Fleming, and S. Mukamel, J. Chem. Phys. **98**, 5314 (1993).
[50] G. R. Fleming, *Chemical Applications of Ultrafast Spectroscopy* (Oxford University Press, New York, 1986).
[51] X. Wei, P. B. Miranda, C. Zhang, and Y. R. Shen, Phys. Rev. B **66**, 085401 (2002).
[52] A. Tokmakoff, A. S. Kwok, R. S. Urdahl, R. S. Francis, and M. D. Fayer, Chem. Phys. Lett. **234**, 289 (1995).
[53] D. E. Moilanen, E. E. Fenn, D. Wong, and M. D. Fayer, J. Am. Chem. Soc. **131**, 8318 (2009).
[54] D. E. Moilanen, D. Wong, D. E. Rosenfeld, E. E. Fenn, and M. D. Fayer, Proc. Natl. Acad. Sci. U.S.A. **106**, 375 (2009).
[55] E. E. Fenn, D. E. Moilanen, N. E. Levinger, and M. D. Fayer, J. Am. Chem. Soc. **131**, 5530 (2009).
[56] B. Pal, Bull. Calcutta Math. Soc. **9**, 85 (1919).
[57] B. Pal, Bull. Calcutta Math. Soc. **10**, 187 (1919).
[58] R. N. Zare, *Angular Momentum: Understanding Spatial Aspects in Chemistry and Physics* (Wiley, New York, 1988).
[59] M.-L. Horng, J. A. Gardecki, and M. Maroncelli, J. Phys. Chem. A **101**, 1030 (1997).

[60] The orientational relaxation time constant of 106 ps is a personal communication from Professor K. B. Eisenthal, Department of Chemistry, Columbia University (7 Feb. 2010) and has been verified by independent measurement in our laboratory. A different value was published by K. B. Eisenthal and co-workers in Ref. 27.
[61] D. A. Pantano and D. Laria, J. Phys. Chem. B **107**, 2971 (2003).
[62] D. A. Pantano, M. T. Sonoda, M. S. Skaf, and D. Laria, J. Phys. Chem. B **109**, 7365 (2005).